Catchment-scale heterogeneity of flow and storage properties in a weathered/fractured hard rock aquifer from resistivity and magnetic resonance surveys: Implications for groundwater flow paths and residence times distributions

J-C. Comte[1,*], U. Ofterdinger[2], A. Legchenko[3], J. Caulfield[4], R. Cassidy[5], J. A. Mézquita González[1]

[1]University of Aberdeen, School of Geosciences, Aberdeen AB24 3UF, UK
[2]Queen's University Belfast, School of Natural and Built Environment, Belfast BT9 5AG, UK
[3]IRD/Université Joseph Fourier, Grenoble, France
[4]Trinity College Dublin, School of Natural Sciences, Department of Geology, Dublin 2, Ireland
[5]Agri-Food and Biosciences Institute (AFBI), Belfast BT9 5PX, UK
*Correspondence (jc.comte@abdn.ac.uk)

Running Title

Flow and storage properties of fractured rocks

Abstract

Groundwater pathways and residence times are controlled by aquifer flow and storage properties, which are characterised by high spatial heterogeneity in weathered/fractured hard rock aquifers. Building on earlier work in a metamorphic aquifer in NW Ireland, new clay mineralogy and geophysical data analyses provided high spatial resolution constraints on the variations of aquifer properties. Groundwater storage values derived from magnetic resonance sounding and electrical resistivity tomography were found to largely vary laterally and with depth, by orders of magnitude. Subsequent implementation of numerical, 2D-hillslope groundwater models showed that incorporating heterogeneity from geophysical data in model parametrisation led to best fit to observations as compared to a reference model based on borehole data only. Model simulations further revealed that; 1/strong spatial heterogeneity produces deeper, longer groundwater flow paths and higher age mixing in agreement with the mixed sub-modern/modern ages (mostly <50 years) provided by independent tritium data; 2/areas with extensive weathering/fracturing are correlated with seepage zones of older groundwater, due to changes in the flow directions, and are likely to act as drainage structures for younger groundwater on a catchment or regional scale. Implications for groundwater resilience to climate extremes and surface pollution are discussed along with recommendations for further research.

Weathered/fractured hard rock aquifers underlie over 20% of the global land surface (Sharp 2014) and are characterised by a high degree of structural heterogeneity and overall low productivity. In recent years, water managers and policy-makers have moved to adopt a catchment scale approach to the integrated management of surface and subsurface water resources (EU Water Framework Directive 2000/60/EC), including the UK (UKTAG 2011) and Ireland (Daly *et al*. 2016). Understanding spatial variations of aquifer hydraulic properties at the catchment-scale, which dictates groundwater flow pathways and residence times, is crucial to inform catchment management plans. Yet, resolving such spatial heterogeneity in fractured bedrock remains very challenging due to the typically scattered nature of direct observations points (boreholes and outcrops) that usually do not have sufficient spatial coverage to capture the scale of heterogeneity (De Marsily *et al*. 2005; Neuman 2005).

To address the lack of spatial resolution in heterogeneous fractured rock catchments, traditional direct testing techniques in boreholes, such as hydraulic testing and geophysical logging, are increasingly combined with indirect and more spatially integrative investigation methods, including tracer testing (e.g. Klepikova 2016), geophysical imaging (ground- or airborne-based) (Comte *et al*. 2012; Shakas *et al*. 2016; Day-Lewis *et al*. 2017) and remote sensing (Cassidy *et al*. 2014; Frances *et al*. 2014). The use of geophysics has long proven effective in resolving, at catchment scale, the heterogeneity of fractured rock aquifers (Holbrook *et al*. 2014; Robinson *et al*. 2016). The Electrical Resistivity Tomography (ERT) method is known to be efficient at imaging spatial variability in weathering, geological heterogeneity and fracture patterns (e.g. Chandra *et al.* 2010; Rainer *et al*. 2007). All ERT studies, however, stress the importance of *a priori* information, especially borehole data and outcrop mapping to support its hydrogeological interpretation (Skinner & Heinson 2004; Comte *et al.* 2012).

A number of studies have demonstrated the benefits of using ERT in combination with other geophysical methods; in particularly with the magnetic resonance sounding (MRS) that complements imaging of heterogeneity by ERT with lower resolution but more quantitative information on water storage. Both methods have, for instance, been used to map groundwater occurrence and develop hydrogeological conceptual and numerical models in weathered basement aquifers (Frances *et al.* 2014; Baltassat *et al.* 2005) and monitor groundwater recharge (Descloitres *et al.* 2008). As yet, however, most of these studies have focused on low latitude regions with deep and relatively water-productive weathering horizons (saprolite) that produce strong MRS and ERT responses for relatively simple, layered aquifer geometries. There are fewer examples in higher latitude catchments with a glacial legacy, such as in Ireland, where most of the saprolite (relatively high storage, porous layer) is absent, exposing only the fractured (low storage) and structurally complex bedrock. In addition, these geophysical approaches still remain either (i) not systematically applied in catchment groundwater studies or (ii) applied qualitatively, i.e. used to inform aquifer heterogeneity conceptual models rather than to quantify spatial variations in aquifer properties (permeability and porosity). This needs further consideration in highly heterogeneous basement rock catchments.

In Ireland, the fractured rock aquifers provide a good analogue of temperate region bedrock aquifers with a glacial legacy. The island of Ireland is underlain by over 60**%** of hydrogeologically poorly-productive fractured bedrock (Moe *et al.* 2010), either cropping out directly or covered by superficial glacio-fluvial and/or alluvial sediments. Most of this poorly-productive bedrock is composed of various grades of metamorphic (basement) rocks; from low-grade metasediments to high-grade gneiss-migmatites and granitoids. Groundwater in these rocks, despite their overall low productivity, is nonetheless crucial for maintaining river base flow during dry periods and supporting aquatic ecosystems and small-scale rural water supply (DCCAE 2017). Over the last decade, the extension of the Irish national groundwater monitoring network to poorly productive basement aquifers as part of implementing the European Union's Water Framework Directive (EPA 2006; Moe *et al.* 2010) has stimulated hydrogeological research through Irish Government-funded projects. Among them, the Griffith Poorly-productive Aquifers Project (2007-2014), on which this work is based, aimed to improve the understanding of groundwater flow regimes in fractured rock aquifers

and the contribution of groundwater to catchment water balance (Comte *et al.* 2012; Cassidy *et al.* 2014; Caulfield *et al.* 2014; Cai & Ofterdinger 2016).

This paper presents an overview of the latest research in a micaschist catchment in Co. Donegal, Republic of Ireland, with the aim of resolving catchment-scale spatial variations of aquifer properties. It synthesises previously published research on aquifer typology and well-scale hydraulics (Comte *et al.* 2012; Cassidy *et al.* 2014), bedrock weathering (Caulfield *et al.* 2014) and aquifer storage properties (Legchenko *et al.* 2017), augmented with the latest results from quantitative interpretation of geophysical data (ERT and MRS) to provide a robust spatial understanding of flow and storage property fields. This work further explores the integration of the existing knowledge on the heterogeneity of aquifer properties using numerical models to assess groundwater flow paths and residence time distributions. Finally, we use the results to discuss the impact of climate change and contaminant transport on groundwater resources and catchment management, as well as further recommendations for improved groundwater modelling.

Hydrogeological setting

Geology

The Gortinlieve catchment (5 km^2), Co. Donegal, NW Ireland (Figure 1) is underlain by Late Precambrian micaschists and psammites of intermediate metamorphic grade (low amphibolite facies). These belong to the Grampian terrane in Co. Donegal as part of the Southern Highland Group, spanning through Ireland and Scotland. They originate from turbidite sequences deposited c. 550 Ma BP (McConnell & Long 1997; Caulfield *et al.* 2014) and subsequently subjected to poly-phase deformation and metamorphism during the Caledonian orogeny. The Caledonian tectonic regime associated with the closure of the Iapetus Ocean (Grampian phase, early Ordovician) generated the current regional NE–SW oriented structures (Chew 2009) characterised by fault scarps and cartographic/topographic lineaments visible in the upper catchment (Fig. 1). The later Taconic phase (late Ordovician) generated the current WNW-ESE orientation deformational structures and imprinted the retrograde amphibolite metamorphic facies (McConnell & Long 1997). The current, Alpine, strike-slip tectonic regime, is reflected by reactivation of NE-SW fracture orientations and further creation of a general NW-SE trend (Worthington & Walsh 2011; Cooper *et al.* 2012). Localised kaolinite rich Tertiary lateritic horizons preserved on Grampian rocks of western Ireland (Legg *et al.* 1985) provide evidence that the basement was during this time at least partially exhumed and undergoing tropical weathering. Subsequent Quaternary glaciations have resulted in further erosion, including the removal of the upper levels of the weathering profiles, most pronounced in high topographic areas, and in the deposition of heterogeneous glacio-fluvial material (clay-till and sand and gravel) in low-lying areas and valley bottoms.

Hydrogeology and borehole instrumentation

Annual rainfall in the area ranges from 1000 to 1200 mm and mean temperature annually ranges from 6 to 14 °C (Met Eireann 2017). The catchment comprises a headwater stream network of a Carrigans River, a tributary of the River Foyle that discharges into the Atlantic Ocean, approx. 40 km NE of the catchment (Caulfield *et al.* 2014). The Gortinlieve catchment was instrumented with monitoring boreholes by the Irish Environmental Protection Agency (EPA) in 2006 as part of the national groundwater monitoring programme. Three borehole clusters were sited in a linear hillslope transect at high (GO1, 174 m above mean sea level; hereafter noted m amsl), intermediate (GO2, 88 m amsl) and low (GO3, 33 m amsl) elevations within the catchment. Individual clusters contain up to 4 boreholes, each isolated and screened across different depth-distinctive zones commonly encountered in Irish bedrock aquifers. The initial classification of Moe *et al.* (2010)

conceptually described these respective intervals as; subsoil SS (average interval 1–3 m below ground surface (bgs); only present in Gortinlieve at the valley bottom), transition zone T (average interval 4–5 m bgs), shallow bedrock S (average interval 8–19 m bgs) and deep bedrock D (average interval 30–67 m bgs). The conceptual model was further refined by Comte *et al.* (2012) in order to help reconcile geological features with geophysical constraints (Fig. 2): overburden deposits (cf. subsoil); broken bedrock (cf. transition zone); fissured bedrock (cf. shallow bedrock); massive bedrock (cf. deep bedrock). The Irish EPA monitors water levels at 15-minute intervals in each borehole using automatic data loggers. The site was also equipped with an automated tipping bucket rain gauge (AEG 100) since October 2010 for the duration of the project.

Aquifer characterisation methods

Structural, mineralogical and hydraulic investigations

Detailed analysis of fracture patterns and clay occurrence in the bedrock was carried out in order to establish the micro- to meso-scale structural controls on groundwater flow, and to provide constraints on larger (meso- to macro) scale hydraulic and geophysical interpretations and numerical modelling.

Fracture orientations were measured on maps, outcrops, boreholes and quarry exposures. Regional structural trends were determined from interpretation of the geological map (Smith 1991; Long et al. 1992; McConnell & Long 1997) and the 20-m resolution digital elevation model (Ordnance Survey of Ireland). During field mapping, the main fracture parameters measured were strike, dip magnitude, dip azimuth with a minimum of 30 fracture measurements for each sample site, subsequently plotted as rose diagram and Schmidt net pole density distribution. The acquisition and plotting methodology are described in details in Comte *et al.* (2012) and Nitsche (2014). Borehole fractures were analysed using acoustic televiewer logs. Among these, hydraulically active fractures were identified through cross-correlation with electrical conductivity logs whereby marked changes in water electrical conductivity at the depth of observed fractures was interpreted as fracture flow (Nitsche 2014).

Mineralogical and petrographic data are summarised by Caulfield *et al.* (2014). Representative field outcrop and recovered borehole core samples were further characterised in this study to quantify the relative proportions of identified phyllosilicate minerals to assess their influence on geoelectrical properties. The mineral modes of the dominant basement lithologies (psammitic schists uphill vs. micaschists downhill) were quantified by petrographic point-counting (500 points per slide). These compositions were taken to represent fresh, primary (unweathered) bedrock. Free phyllosilicate minerals (mineral grains not bound in the competent fresh bedrock structure) were separated and collected from weathered samples by repeated washing with distilled water and dried at 50°C. Clay sized (<2 µm) fractions were obtained following the method outlined in Caulfield *et al*. (2014), and references therein. The relative proportions of primary (muscovite, chlorite) and secondary (illite, montmorillonite and illite/montmorillonite admixtures) were determined via thermogravimetric analysis (TGA) using a Netzsch libra thermogravimetric analyser, in conjunction with XRD and FTIR results from Caulfield *et al*. (2014). Samples were heated from 200-880°C to determine sequential dehydroxylation water loss from the clay mineral fraction. Mineral proportions (volume %) were converted to weight %. Using the method of Revil *et al*. (1998), the total cation exchange capacity (CEC) of the different geological units (transition, shallow, deep bedrock) at each of the three sites (GO1-3) were calculated from (i) the relative mass proportion of clay minerals, (ii) their individual CEC, obtained from literature (Swineford 1955; Carroll 1959; Wiklander 1964; Thomas 1976; Ridge 1983; Revil *et al*. 1998; Crain 2000; Gillespie *et al*. 2001; Ellis & Singer 2007; Henn *et al*. 2007) and (iii) the total clay content derived from natural gamma ray logs from each borehole.

Aquifer pumping and recovery tests were implemented in every borehole to provide local values of equivalent hydraulic conductivity and storativity for each borehole. The hydraulic testing methodology is described in details in Comte *et al*. (2012). Pumping test were conducted at a constant rate (2 to 30 L/min depending on the borehole) and both pumping and recovery curves were jointly interpreted using AQTESOLV Pro v4.5 and applying a range of adapted analytical solutions (with regards to the known aquifer structure and the borehole technical characteristics) including single porosity/permeability models. Hydraulic conductivities (*K*) were calculated from transmissivity values using observed unit aquifer thicknesses from borehole data, ERT data and geophysical logging data.

K in fractured rocks is typically anisotropic, i.e. directionally dependent implying different *K* values in different directions, with the maximum hydraulic conductivity *Kmax* following the direction of the hydraulic active fractures and the minimum hydraulic conductivity *Kmin* being orthogonal to the hydraulic active fractures. This further implies that the anisotropy angle in fractured rocks, because of the presence of steep fractures, has a higher vertical component than in most sedimentary rocks where the direction of *Kmax* is often sub-horizontal, parallel to the sedimentary bedding (in this case *Kmax* is usually denoted *Kh*) and the direction *Kmin* is subvertical (and in this case denoted *Kv*). In this work, values of hydraulic conductivities provided by hydraulic tests were further analysed in terms of anisotropy in 2D (along the studied transect). As hydraulic test values were assumed equivalent to isotropic hydraulic conductivities, the integration of fracture analysis data allowed for the definition of *Kmax* *Kmin* and anisotropy angles (by definition the angle of *Kmax* to the horizontal) based on the measured orientation of the hydraulically active fractures. The anisotropy ratio *Kmin*/*Kmax* (unitless) was derived by considering it to decrease with depth from 0.5 to 0.1. At depth, where the steep fracture sets dominated (see section *Aquifer characterisation results*) and produced a stronger anisotropy, the ratio was set to 0.1, whereas at shallow depths, where other fracture sets and pronounced weathering contribute to flow, particularly in the broken bedrock, anisotropy was expected to weaken and was therefore set to 0.5. The anisotropy angle was derived as an average of the individual angles of the dominant fracture sets for each bedrock conceptual unit (broken, figured, massive).

Geophysical investigations

Electrical resistivity tomography and petrophysical models for porosity estimation

A geophysical survey using electrical resistivity tomography ERT was carried out to provide a catchment-scale conceptual understanding of the bedrock heterogeneity and its hydrogeological significance. ERT was applied along the hillslope transect of the three well clusters using a Syscal Pro 72 resistivity meter. As described in Comte *et al*. (2012), the acquisition was carried out with 60 electrodes at 5-m unit electrode spacing, subsequently expanded through roll-along. The dipole-dipole (DD) and multi-gradient (mGD) quadripole configurations ran sequentially, ultimately allowing a depth of investigation of 50–60 m (Edwards 1977). After noise removal, DD and mGD apparent resistivity data were jointly inverted using RES2DINV v3.58. The inversion provided a 2D model of specific resistivities in which model regions that are insensitive to the input data were removed using the depth of investigation (DOI) method of Oldenburg & Li (1999). The best model retained for hydrogeological interpretation was obtained for the 5th iteration, giving an absolute error between observed and calculated apparent resistivities of 9.6%.

In addition to the structural information provided by the interpretation of spatial resistivity variation, a petrophysical model was applied to the resistivity model in order to derive bedrock porosity. Due to the substantial amount of clay minerals (both primary and secondary) in the psammites and the micaschists, Archie's model (Archie 1942) was not applicable and instead, the Waxman and Smits (1976) model was used. The Waxman and Smits model relates the bulk (specific) resistivity obtained by inversion to the aquifer total porosity (which is the unknown to resolve), the

pore water saturation (equal to one below the water table), the rock matrix cementation factor, the groundwater electrical conductivity and temperature, and in addition to Archie's Model, the total rock CEC, which was obtained from mineralogical investigations and natural gamma logs (see section *Aquifer characterisation results*). The model is described in Revil et al. (1998) and was applied to estimate the 2D (hillslope) distribution of total porosity along the transect imaged by ERT. Table 1 summarises the values of the parameters used for the different hydrogeological units.

Magnetic Resonance Sounding

The magnetic resonance sounding (MRS) method (Legchenko 2013) was applied at 11 points along the ERT transect and close to the borehole clusters (Fig. 1). The MRS surveys provided 1D (vertical) profiles of water content. MRS measurements were performed in two surveys, in 2010 and 2016 using the NUMISPLUS and NUMISPOLY instruments, respectively, both developed by IRIS Instruments (France). As described in more detail in Legchenko *et al*. (2017), figure-eight square loops were applied in three configurations: two cable turns of 25-m-side, one turn of 37.5-m-side, and one turn of 50-m-side, with a reference loop in 2016 to improve the signal to noise ratio, which is typically low in fractured rock environments, due to a low water content. Eight out of the 11 MRS soundings had acceptable signal-to-noise ratios; the remaining three are not considered in this work. 1D inversion of MRS data was carried out using the SAMOVAR software package. It used the Tikhonov regularization method (Legchenko & Shushakov 1998) and the uncertainty in the inversion results was examined applying Monte-Carlo simulations (Legchenko *et al*. 2017). Geological interpretation of MRS results was performed taking into account the thicknesses of the aquifer units (broken and fissured zone) identified with ERT as structural constraints.

Estimation of aquifer storage parametres from ERT porosity and MRS water content

ERT porosity and MRS water content were used to derive aquifer specific yield *Sy* and effective porosity n_e subsequently used for recharge estimation, and numerical groundwater modelling, respectively. By definition, n_e is the interconnected porosity controlling groundwater mass transport and residence times. Also by definition, *Sy*, also called drainage porosity, is the mobile pore water not retained by capillarity forces and controls water table fluctuations in unconfined aquifers.

In fractured rocks, where porosity is mostly the result of the opening of fractures and foliation planes by (groundwater-aided) weathering, the occurrence of closed (unconnected) pore space is limited (Singhal & Gupta 2010). This implies that total porosity, obtained from ERT, can be considered a close estimate of the effective porosity n_e, which was our assumption for subsequent modelling.

The MRS water content is commonly reported (Lubczynski & Roy 2004) as being correlated with, and representing an intermediary between, the drainage porosity *Sy* (mobile pore water non retained by capillarity forces) and the effective porosity n_e (immobile and mobile interconnected pore water). Recent studies carried out in low porosity fractured environments (Vouillamoz *et al*. 2012, 2014) have reported MRS water content values linearly correlated to, although higher than *Sy* (within a factor 2) estimated through pumping tests. Consequently, for subsequent recharge calculations we have taken *Sy* at half (0.5 times) the measured MRS water content.

Recharge estimations

Recharge values were calculated with the water table fluctuation method applicable to recharge estimation in unconfined aquifers (Healy & Cook 2002). The method requires water table time-series as well as well as values of the specific yield at depth where the water table fluctuates. We used the piezometric fluctuations in the shallowest boreholes (GO1T, GO2T and GO3SS) as reported in Cai & Ofterdinger (2016) for the period 2010-2012. For the specific yield, we used the MRS derived values

obtained at the approximated depth of the water table (see previous Section) from the MRS soundings nearest to the boreholes; MRS1 and MRS2 for GO1T, MRS4 and MRS5 for GO2T, and MRS8 for GO3SS.

Aquifer characterisation results

Aquifer structure and weathering

Fracture analysis

Measurements of hydraulically active fracture from both outcrops and boreholes at the site showed dominant meso-scale (millimetre to metre) fracture occurrences and orientations which correlate with established past tectonic regimes in Ireland (Fig. 3). Two dominant hydraulically active fracture sets were identified: a dominant set with fractures oriented E-W to NE-SW with a dip angle of about 60-80° S to SE; and a less frequent set with fractures also oriented E-W to NE-SW but with a dip angle of about 60-90° N to NW. The dominant fracture set may be attributed to the strike-slip regional fracturing associated with Alpine compression during the Palaeocene, whereas the second set may be attributed to the compressive fabric of the Neo-Proterozoic to late Carboniferous orogenies (Grampian, Caledonian and Variscan), which also characterise the regional-scale lineaments (Fig. 1) and Lower Carboniferous normal faults (Worthington & Walsh 2011), reactivated by the Alpine strike-slip regime (Cooper *et al*. 2012). The most frequently recorded fracture set is oriented WNW–ESE with a low dip angle of 35 ° NNE corresponding to the highly weathered Dalradian schistosity plane (see below). However, this set does not appear to be clearly associated with hydraulic activity in boreholes and therefore may only play a role in the uppermost levels of the aquifer (broken bedrock and possibly the upper part of the fissured bedrock) for which hydraulic activity in boreholes is difficult to record due to their shallow depths and denser weathering/pervasive fracturing.

At macro-scale (catchment and regional scale, i.e. 100 m to km; Fig. 1b), cartographic lineaments attributed to glacial erosion preferentially affecting regional geological boundaries and deep weathering corridors were found to be typically associated with the measured pre-Alpine NE–SW trend (Comte *et al*. 2012).

Mineral analysis

Mineralogical investigations reveal that phyllosilicate minerals are dominated by muscovite and chlorite (primary) and illite and montmorillonite (secondary clays produced by weathering of chlorite and muscovite) (Caulfield *et al*. 2014). Major non-clay minerals comprise quartz and feldspar.

Relative proportions of clay minerals versus the total clay mass fraction are presented in Table 2. The massive (unweathered) bedrock encountered in the deep boreholes was found to contain negligible secondary clays, with only primary chlorite and muscovite observed. The fissured zone in boreholes GO2 and GO3 contained an approx. equal mixture of illite and montmorillonite with lesser amounts of chlorite and muscovite, and in GO1, relatively even quantities of the four minerals. This suggests a moderate weathering of the fissured zone primary clays in GO1, whilst in GO2 and GO3, they have undergone major weathering as evidenced by the almost complete absence of chlorite. Over 80% of clays in the broken zone were muscovite and the remaining 20% approx. equal proportions of illite and montmorillonite. Because weathering is most active in the broken zone, it was concluded that secondary clays are transported in suspension downward from the broken zone and redeposited in the underlying fissured zone (Comte *et al*. 2012; Caulfield *et al*. 2014).

Table 2 also details the total clay mass fraction as derived from natural gamma ray logs. The relative proportions of clay minerals and the total clay mass fraction allowed calculation of the total CEC of the different aquifer units using the model of Revil *et al*. (1998). The total clay content of the

different aquifer units (broken, fissured and massive bedrock) was not significantly different; however due to significant differences in clay mineralogy, the resulting CEC is different. The fissure bedrock, with a higher proportion of illite and montmorillonite (secondary weathering clays characterised by high CECs) consistently produced the highest bulk CEC values. The massive bedrock dominated by muscovite and chlorite (primary clays characterised by low CEC values) produced the lowest bulk CEC. This CEC distribution is relevant to the interpretation of ERT results and application of the petrophysical models in which it is a key input parameter.

Geophysical structure

Results of the ERT investigations provide cross-sectional variations of electrical resistivity along the borehole hillslope transect (Figure 4), revealing a high degree of aquifer heterogeneity. As electrical resistivity is primarily controlled by porosity (fracture porosity in the present context), clay content and mineralogy, its spatial variations can be interpreted as reflecting changes in lithology, pore water saturation, open fracture density and weathering intensity. Resistivity values range from about 100 ohm.m to just under 10 000 ohm.m, i.e. three orders of magnitude. Highest resistivities (>> 1000 ohm.m) were observed at the base of the transect and reflect the massive micaschist unit beneath the weathered front, characterised by a low density closed fractures and small quantities of secondary weathering clays. Some equally high resistivity values were also obtained in the very shallow subsurface in the higher elevation part of the profile. Correlations with the depth of the water table in borehole cluster GO1 and observed spring lines at its base suggested that this uppermost, high resistivity unit corresponds to unsaturated, clay-poor psammite-schist. The lowest resistivity values (<500 ohm.m) were obtained at a relatively shallow depth in the flood plain and corresponded to the clay-till and alluvium overburden. Intermediate resistivity values (500-2500 ohm.m) were observed throughout the whole transect at shallow to intermediate depths (0 to about 50 m below surface) and characterised the heterogeneous weathered/fractured schists (broken and fissured bedrock). The relatively continuous unit with values ranging ~300-1000 ohm.m overlying the massive bedrock are interpreted as fissured bedrock characterised by a high density of open fractures possibly filled with high-CEC weathering clays as suggested by the clay mineralogy. This fissured layer was particularly deep at three locations along the transect; at the following horizontal distances from NW end of the profile of X=400-500 m, 750-850 m and 1100-1300 m. Since they correlate well with the regional Grampian lineaments (Fig. 1), these locations are interpreted as deep fractured zones that facilitate deep weathering. At these three locations a slightly more resistant layer was observed overlying the fissured layer, with resistivities in the range of 500-2500 ohm.m. This unit is interpreted as the broken schists (transition zone) where the weathered clays have been leached and transported to the underlying fissured zone.

Flow properties

Pumping and recovery tests in every borehole provided estimates of (equivalent isotropic) hydraulic conductivities *K* for bedrock and overburden (Table 3). A clear trend of decreasing hydraulic conductivity with depth is observed. The broken bedrock (transition zone) displayed mean values close to 10^{-1} m/d, the fissured bedrock close to 10^{-2} m/d with large variability of over two orders of magnitude and the massive (deep) bedrock around 6 x 10^{-3} m/d. The overburden (glacio-fluvial and alluvium deposits) present in the valley floor displayed much higher mean *K* values of ~9 m/d. These values partly agree with values from previous hydraulic tests by Moe *et al*. (2010). These authors obtained much higher mean *K* for the broken bedrock due to one very high value (of about 7 m/d) obtained in the valley floor at GO3, which may be representative of the interface between the overburden glacio-fluvial deposits and the bedrock. They also provided values for the deep massive bedrock that are similar to those in the overlying fissured (shallow) bedrock.

Kmax, *Kmin* and the anisotropy angles (angle of *Kmax* to the horizontal plane, in °) in the 2D vertical plane of the studied transect were further derived based on the measured orientation of the dominant, hydraulically active fracture sets (see previous Section); a primary set ~70° dipping SSE and secondary set ~75° dipping NNW, and another set ~35° dipping NNW which is not clearly hydraulically active at large depths, but is probably active in the weathered near-surface. The anisotropy ratio *Kmin*/*Kmax* (unitless) was assumed to decrease with depth from 0.5 to 0.1 (see Section *Methods*). The calculated anisotropy angle increased with depth from a relatively low angle in the broken bedrock as a result of the equal contribution of the three fracture sets (75° NW) to a dominant steep angle in the deep bedrock (70° SE, parallel to dominant hydraulically active Variscan-Alpine fabrics). Fig. 5 plots the values of *Kmin*, *Kmax* along with the previous equivalent isotropic *K* estimates (Moe *et al*. 2010; Comte *et al*. 2012). The values of *Kmax* were close to the values obtained from hydraulic tests, which were assumed to preferentially mobilise groundwater from the fractures responsible for *Kmax* (direction of maximum anisotropy).

Storage properties

Quantitative information on the heterogeneity of aquifer storage properties was provided by the joint analysis of hydraulic test results and geophysical data (MRS and ERT). Hydraulic test results are limited to single estimates of specific yield (*Sy*). Moreover, *Sy* values obtained from measurements in pumped wells in absence of observation wells are usually inaccurate due to possible well bore storage effects. However they did provide indicative orders of magnitude as a guide, with broken bedrock displaying *Sy* values around 3-5 %, fissured bedrock of about 0.1 % and massive bedrock around 0.001 %, i.e. over an order of magnitude decrease between each layer with increasing depth.

Geophysical data provided higher resolution spatial information on the variability of storage properties. MRS, despite an instrumental sensitivity that currently does not reliably quantify less than 1 % water content, detected appreciable quantities of water above 2% in the central and low part of the transect (Fig. 6). The highest water contents were detected at MRS8 in the valley floor with values between 2 and 6 % at shallow depths (0-25 m) corresponding to the occurrence of the relatively porous overburden materials and the broken bedrock. Similar water content values were also obtained at MRS4, upslope of GO2, at depths (2-15 m) consistent with the area of deep weathering identified by ERT (X=400-600 m on Fig. 4) and characterised by significant deepening of the broken bedrock layer. In the upper part of the transect around GO1, no appreciable water content was detected by MRS suggesting water content < 1 %. This is also the case for the two soundings carried out between GO2 and the valley floor. Overall, the MRS results show relatively good agreement with the depth delineation of the broken bedrock and overburden layers from ERT (Fig. 6 and 7a,b). For the overburden in the valley floor, MRS water content values of approx. 5-6 % were obtained while the broken bedrock (transition zone) yielded values of 2-4 %. At depth below the base of the broken layer (as delineated with ERT), MRS mostly provided either water content values below the normal limit of detection of the methods (1 % water content) or values with high inversion uncertainty. This suggests that the fissured and massive bedrock had water content values < 1 %. Note that the broken bedrock, which is likely present in the upper part of the transect was mostly unsaturated in the summer (dry) conditions when both ERT and MRS surveys were undertaken.

The Waxman and Smits model (Fig. 7c), provided spatial variations of (effective) porosities consistent with MRS results, and porosity values of about half the MRS water contents. Values ranging from 3-7 % were obtained in the overburden/broken bedrock of the valley floor while the broken layer of the mid and upper part of the transect displayed values ranging from 1 to 3 %, decreasing with distance to valley floor. For the fissured layer, we obtained values between 1 % beneath the valley floor to less than 0.1 % in the upper part of the transect, with a relatively progressive decrease from valley bottom to hilltop. Porosities lower than 0.03 % were obtained in the massive, unweathered bedrock layer. As a comparison, Archie's model (not presented here),

which is applicable in clay-free materials, provided much higher, unrealistic porosity values of about an order of magnitude (i.e. about ten times) higher, ranging 1 to 40 %. This confirmed that Archie's model is not applicable in this type of environment due to significant clay content.

The slightly lower (effective) porosities values obtained from the Waxman and Smits model as compared to the MRS water content values, of approximately a factor of two, are consistent with the findings from Vouillamoz *et al*. (2012, 2014) who reported similar difference factors in low porosity (< 3 %) clay-rich bedrock aquifers. This supports the assumption, used for subsequent modelling of residence times, that bedrock effective porosities may reasonably be assumed as equal to Waxman and Smits porosities.

Aquifer recharge

Application of the water table fluctuation using *Sy* values derived from MRS provided recharge values that vary along the hillslope (Table 4), from an average of 163 mm/y in the hillslope to an average of 287 mm/y in the valley bottom, which correspond to about 10% and 20% or the rainfall, respectively. These values are higher than previous values reported by Cai & Ofterdinger (2016) due to estimated *Sy* values higher than the literature values used by previous authors.

Data integration and numerical groundwater modelling

Methods

A 2D numerical groundwater model (equivalent porous medium EPM) was constructed in line with the ERT transect in order to assess the influence of the structural heterogeneity, i.e. the spatial variations in flow (permeability, anisotropy) and storage (porosity) properties on groundwater flow paths and residence time. EPM models are commonly used for studying groundwater dynamics in fractured bedrock aquifers at catchment and hillslope-scale (Ball *et al*. 2014; Welch & Allen 2014; Kolbe *et al*. 2016). EPM models use integrated hydraulic properties data (hydraulic conductivities, storativities) from hydraulic test solutions and anisotropy analysis (which are also EPM models). They are also a lot less computationally expensive than discrete fracture network (DFN) models for which the current hillslope-scale knowledge on the actual distribution and properties (length, aperture, roughness) of fracture networks is insufficient for DFN model application.

We used the finite element code FEFLOW v6.2. The model domain was 2D vertical (cross section; Fig. 8) with a length slightly shorter than the ERT transect (1200 m; the ERT region south of the river was not included). The ground surface was obtained from the DEM and therefore identical to the ERT profile. The maximum elevation (NW of transect) was 183 m and the minimum river elevation (SW of transect) was 31.5 m, i.e. the elevation of the river. The base of the model was fixed at -50 m relative to mean sea level. The mesh comprised 5366 triangular elements and 2974 nodes.

The model domain was structured in five layers: alluvium (only present in the floodplain), broken bedrock, fissured bedrock, massive bedrock, and a hypothetical very low conductivity/porosity bottom layer (Figure 8), within which homogeneous hydrogeological parameters were applied. Two alternative numerical models were applied using different levels of hydrogeological knowledge of the site (aquifer structure, hydraulic properties, and recharge). Model 1 used the information obtained from boreholes only. It considered a uniform layered structure defined from lateral interpolation of the hydrogeological units as identified in boreholes and initially interpreted by Moe *et al*. (2010) prior to extensive deployment of geophysical surveys. This model represents the common, most simple catchment/regional scale conceptualisation of basement aquifers (Fig. 8a). Model 2 incorporated the additional knowledge obtained from the interpretation of geophysical surveys (Fig. 8b). Comparing the two models aimed at illustrating the added value provided by the geophysical data. Details of the set up of both models were as follows.

Model 1 considered a tabular spatial distribution of the different aquifer units that mimics the topography (Figure 8a). Recharge values were based on borehole-based estimates by Cai & Ofterdinger (2016). Model hydraulic conductivities and porosities were assigned from layer-specific hydraulic test results from Moe et al. (2010) and Comte *et al*. (2012), respectively (Table 5). Effective porosities, used for residence time calculations, were assumed to be equal to the specific yield values (*Sy*) from borehole data. As Model 1 initially provided a poor fit to observed groundwater heads, a recalibration had to be performed through increasing recharge (x5) and decreasing hydraulic conductivities (/5).

Model 2 was based on the geometry of the different aquifer units from the interpretation of the geophysical data (ERT and MRS). Recharge values were the new values calculated with the water table fluctuation method using the specific yield data derived from the MRS surveys (see Section *Aquifer characterisation*). Hydraulic conductivities *K* (Table 5) were applied as anisotropic and assigned from joint interpretation of revised hydraulic test data Comte *et al*. (2012), geophysical data and fracture analyses (see Section *Aquifer characterisation*). Effective porosities (Table 5) were assigned using the porosity values obtained from joint application of ERT and MRS (Figure 7 and Table 5).

Both models were assigned values of longitudinal and transversal dispersivity of 30 and 3 m respectively, as typically reported for fractured aquifers for the scale of this study (hundreds of m to km-scale flow paths; Neuman 2005; Schulze-Makuch 2005; Zhou *et al*. 2007). With regard to the boundary conditions other than the recharge described above, both models also computed the top surface as a seepage face, with recharge (entering flux) switching automatically to discharge (exiting flux) during simulations when the water table was equal or higher than the top surface. Additionally, the river was applied as a constant head of 31.5 m, which is the average observed river level. In terms of groundwater ages, water entering from recharge was assigned a constant age of 0 years.

Models were run in transient flow and age conditions with initial heads equal to the topographic elevation and initial ages of 0 years, until reaching a dynamic steady state. Flow and groundwater age were solved simultaneously. Groundwater age simulations in FEFLOW are treated as dissolved transport and account for the applied values of effective porosities and dispersivities. This, contrary to isochrone calculations on flow paths (streamlines), allows for water dispersion and mixing of groundwater ages. Flow path simulations were run on simulated flow fields to highlight average flow paths from recharge (top surface) to discharge points (river and seepage areas).

Numerical modelling results

Models evaluation

The goodness-of-fit of the different models, i.e. the discrepancy between predicted and observed heads was assessed through root-mean-square error (RMSE) calculations. Model 1, which computed previously published values of hydraulic properties (Moe *et al*. 2010) and recharge (Cai & Ofterdinger 2016) initially failed to reproduce hydraulic heads that fit the observed head in the boreholes. Calculated head values were significantly lower than observed, of up to 125 m difference at GO1 (uphill), due to either underestimation of the recharge or overestimation of the aquifer hydraulic conductivities, but close to observations downhill due to the constraint by the river fixed head. Across the whole transect this model produced a high total RMSE of 71.6 m. The recalibration of Model 1, through increasing the recharge and decreasing *K* both by a factor five, produced a reasonable fit with a RMSE of 3.7 m. Models 2 directly reproduced reasonably well the hydraulic heads observed in the boreholes GO1, GO2 and GO3 with a RMSE of 4.0 m. For Model 2 however, the simulated heads in the deep GO1 and GO2 boreholes were somewhat higher than those

observed. Because these two boreholes are within or close to deep weathered/fractured zones (as identified by geophysics), a 3D model allowing deep and lateral drainage would be expected to correct for this mismatch by lowering heads in the deep units. The model comparison demonstrates that both Model 1 (final recalibrated version) and Model 2 equally honour the observed heads, however only Model 2 also honours the observed aquifer properties, structure and recharge values.

Simulation of groundwater fluxes, flow paths and residence time distributions

For both Model 1 and Model 2, Darcy's fluxes were highest in the broken bedrock and decreased with depth (Fig. 9a,d). The deep weathered/fractured zones identified by geophysics and computed in Model 2 allowed for thicker areas of high flux (Fig. 9d), especially in the vicinity of these zones (X 300-600 m; 750-850 m; 110-1300 m). In terms of budget (Fig. 10), in the case of Model 1 almost 80 % of the flow rate in the aquifer, originating from the recharge, transited through the broken bedrock layer (transition zone) and fissured layer (shallow zone), with over 60% in the broken bedrock only. The proportion was lower for Model 2, with about 70% flowing through broken and fissured bedrock and about 50% through the broken bedrock only. This suggests that overall hydrogeological heterogeneity favours deeper groundwater flow in the fissured and massive bedrock (< 20 % for Model 1 vs. about 25 % for Model 2).

This is further confirmed by the average flow path (streamlines) simulations (Fig. 9b,e). In the case of Model 1, most flow paths were sub-horizontal and restricted to the shallow broken layer (Fig. 9b). A limited number of flowlines travel through the fissured and massive layers. For Model 2, which incorporated lateral variations in the thickness of the aquifer layers, flow paths were more evenly distributed with depth, with higher contributions from the fissured and massive layers (Fig. 9e). They were also characterised by undulations as a result of lateral variations of weathering thicknesses and the anisotropy of conductivity with an increased vertical component to the groundwater flow. In detail, Model 2 simulations showed sub-vertical or oblique groundwater flow from recharge locations where weathering/fracturing is poorly developed. In locations with extensive weathering/fracturing, groundwater directions changed upwards suggesting that these locations may act as drainage structures at catchment and regional scale. These model regions were also associated with groundwater discharge through seepage, which agree with the spring lines locations observed in the field (Fig. 4). Seepage appeared to occur specifically in areas where the two following conditions are met: (1) upwelling groundwater flow associated to decrease in thickness of the broken bedrock on the downgradient side of deep weathered/fractured 'channels' and (2) presence of topographic low also associated to less competent bedrock in these zones. In contrast the absence of deep weathering zones in Model 1 resulted in higher and more evenly spread seepage along the hillslope.

Groundwater age simulations for the two models (Fig. 9c,f and Fig. 11) provided ages increasing both laterally from hill top to the valley and with depth. Youngest groundwater was obtained in GO1T and GO3SS and oldest in GO3S, GO3D and GO2D (Fig. 11). Model 1 and Model 2 both resulted in simulated ages less than about 10 years and 50 years, respectively, in boreholes and seepages areas. When compared to Model 1, which did not incorporate lateral heterogeneity, Models 2 showed greater age mixing with depth whereas the former produced steeper age gradient with depth in the upper aquifer. Model 2 ages are consistent with independent Tritium data (Pilatova 2013) that showed (1) Tritium concentrations in boreholes within the range 2.5-17.6 TU reflecting a mixture of sub-modern water (< 1TU; prior 1952) and modern water (5-15+ TU, i.e. < 5 to 10 years) (Figure 11), (2) decreasing Tritium values with depth reflecting larger component of older waters with depth, (3) highest Tritium values (>14 TU) in the upper bedrock at GO1T well (X=~100 m) and GO2S well (X=~600 m) reflecting high proportion of young water associated to recharge as well as descending to sub-horizontal groundwater flow and (4) lowest Tritium values (2.5 TU) encountered at the deep GO3D well (X=~1200 m) reflecting larger component of older upwelling groundwater.

The distribution of residence times obtained for Model 2, the best parameterised model accounting for the geophysical heterogeneity, is also broadly consistent with previous catchment- or

hillslope-scale studies in fractured hard rock aquifers. Robins & Smedley (1994) reported modern groundwater tritium ages in the fractured basement of Jersey. Jaunat *et al*. (2012) reported CFC-SF6 residence times lower than 50 years in weathered/fractured gneiss of the French Basque Country for similar flow path lengths. Banks *et al*. (2009) reported CFC ages of less than 40 years in a hillslope transect underlain by weathered/fractured metasediments. Lapworth *et al*. (2013) reported CFC-SF6-3H mean residence times of 32-65 years in deeply weathered catchments of the West African basement. Kolbe *et al*. (2016) modelled mean transit times of 40 years in a granite-gneiss catchment of ~10 km-long with similar mean flow path lengths of ~300 m. The modelling results also corroborate recent findings by Ameli *et al.* (2016) who showed the major impact of subsurface heterogeneity on groundwater residence time distribution in a well-studied hillslope transect in glacial till in Sweden.

General discussion

Study implications for groundwater resilience to climate change and contaminants, and catchment management approaches

The results indicate that overall low and depth-decreasing porosities, together with high hydraulic gradients, give relatively short residence times for groundwater from recharge to seepage or river discharge. In the upper bedrock (broken bedrock/transition zone; 1 to 30 m thick), where over 50% of groundwater flow occurs, models results suggest groundwater flow paths of between 10-100 m long and groundwater ages of < 1 year. This implies that groundwater in this aquifer unit is sensitive to both weather seasonality and extreme events (winter/summer recharge condition and drought/floods). This groundwater mostly contributes to diffuse seepage, which is then collected by agricultural drains. As such, point and diffuse contaminants in groundwater are expected to affect surface water quickly, on timescales of days to months. In the deeper bedrock (fissured/shallow and massive/deep bedrock; depths higher than 10-50 m), model results yield longer flow paths (100-1000 m) and older groundwater ages (from one year to several decades). This implies higher groundwater resilience to extreme weather conditions, seasonality and incidental contaminant exposures, but not to long-term (multi-decadal) climate change and persistent contamination, such as (i) changes in recharge due to long-term changes in rainfall and evapotranspiration and (ii) diffuse (e.g. agricultural nutrients) contamination. As these deeper bedrock units mostly contribute to river flow as well as the most significant seepages areas/drains, the surface water network at base flow (i.e. when mostly supported by groundwater) is also expected to be more vulnerable to long-term climate change and contamination.

Model comparison (Model 1 vs. Model 2) further highlights the importance of adequately accounting for aquifer heterogeneity when using models to predict the response of weathered/fractured rock catchments to climate and land use change as well as contaminations. Using information from borehole observations only, which does not allow for adequately capturing spatial variations in weathering/fracturing, leads to underestimation of the contribution of deep aquifer units to catchment water balance and discharge to river/surface water bodies. This also leads to underestimating groundwater residence times and exaggerating both ground and surface water sensitivity to climate variability and contaminations. In contrast, better accounting for aquifer heterogeneity as revealed here by geophysical surveys, results in higher resilience of groundwater resources to climate variability and surface contaminations. This is of importance when applying groundwater models with the aim of accurately informing short to long-term catchment management and policy.

Study limitations and implications for residence time distributions

The hydrogeophysical and numerical modelling works conducted in this study reveal the major role played by hydrogeological heterogeneities on groundwater flowpaths and transit time distributions at 2D hillslope scale providing important insights into catchment scale groundwater processes in weathered/fractured aquifers. The methodology however has some limitations with respect to accurately representing 3D heterogeneities and their influence on flow and transit times at smaller (i.e. borehole) or larger (i.e. catchment or region). Specifically, the hillslope characterisation and modelling work conducted do not represent; (1) three-dimensional groundwater flow such as lateral or deep drainage due to deep weathering structures possibly significant at the catchment/regional scale; (2) individual fracture networks and associated fracture flow processes; (3) accurate 2D/3D clay distribution and cementation factor; (4) uncertainty in estimates of hydrogeological porosity from geophysical (ERT and MRS) porosity; (5) temporal variability in recharge; (6) flow processes in the unsaturated zone above the water table.

With regards to the two-dimensionality of the models, it may be expected that some groundwater flow at the catchment scale may take place laterally to the 2D transects especially (i) in deep weathering furrows such as these detected by geophysics at about 300-600m, 750-850m and 110-1300m; (ii) in more local preferential flow paths along the NE-SW fractured systems. Not accounting for these 3D processes, the current modelling approach is likely to lead to underestimate deep groundwater flow as well as mixing and resulting groundwater ages, and overestimate seepage (along the hillslope). Full 3D geophysical (acquisition and inversion) and numerical modelling approaches are recommended in basement catchments where strong 3D heterogeneity is expected. The expected increased accuracy is however at the cost of much higher requirement in terms of acquisition and modelling time and resource, including computational.

Increased accuracy in modelling results may also be obtained by implementing discrete fractured network (DFN) modelling approaches. The structural and geophysical data may be used to support the computation of fracture orientation and density, which would allow direct computation of fracture permeability and aperture. A DFN approach requires implementation of computationally expensive 3D models.

Application of ERT to derive porosities requires information on spatial variations of bedrock clay content and clay mineralogy. Direct and high resolution 3D characterisation of clay properties through sampling/coring is challenging, but such resolution may be achieved indirectly through use of alternative geophysical methods such as the induced polarisation (IP).

In line with previous works in similar settings, we have assumed that aquifer effective porosity was half the MRS water content and equal to ERT porosity. Should this assumption be erroneous, effective porosity values higher than the ERT total porosity would result in higher groundwater residence times. More research is recommended to constrain the relationship between ERT/MRS porosity and hydrogeological porosities (storativity and effective porosity).

The temporal variability in recharge has not been accounted for and would be required to better understanding seasonality in groundwater contribution to seepage, drains and stream. It may, in addition, enhance groundwater mixing and, therefore groundwater residence times. Similarly, neglecting flow processes in the unsaturated zone primarily result in underestimating groundwater mixing and ages in areas where the unsaturated zone is thicker.

Conclusion

The study highlights the strong control of geological heterogeneities on groundwater flow and residence times in metamorphic rock catchments in temperate regions. It also demonstrates the high value of surface geophysical data and fracture and clay analysis for the parametrisation of numerical groundwater models in complex aquifers.

The investigations have revealed a high degree of heterogeneity in the distribution of hydrogeological properties at the hillslope scale. Through 2D equivalent porous media modelling using FEFLOW, it has been shown that the high spatial variation of hydraulic conductivity and porosity results in deeper groundwater flow paths (with an increased in the vertical flow component with depth) as compared to simple layered conceptual models based on borehole data only. They also result in older groundwater ages through enhanced mixing and dispersion caused by heterogeneities and anisotropies of hydraulic conductivity. Groundwater ages along the hillslope were simulated to be of modern ages, i.e. less than 50 years, consistent with available Tritium data.

The integrated approach presented, using both borehole and surface geophysical surveys, is shown to help parametrise numerical groundwater models that honour the observed data without requiring significant parameter recalibration. Such robustly parameterised models offer straightforward application in catchment water management, to investigate in detail the contribution of groundwater to the catchment hydrological function, as well as the impact of climate change and contaminants on groundwater.

The results presented here suggest that the uppermost weathered/broken part of the aquifer, which is a major contributor to hillslope discharge, is sensitive to extreme hydrological events and seasonal climate fluctuations as well as point and diffuse contamination. The deeper, less weathered part of the aquifer is a significant contributor to river flow and major hillslope seepage areas and would be more sensitive to long-term (decadal) climate fluctuations and persistent, diffuse contaminants.

It is suggested that the 2D steady-state hillslope approach conducted provides only a minimum estimate of groundwater ages at the catchment scale. This is due to underestimation of groundwater mixing favoured by possible 3D structures and seasonal recharge. Full 3D characterisation and modelling approaches, although more expensive in terms of data and computational resources, are required to further improve our understanding of groundwater flow and residence times. Recommendations include: (1) implementation of 3D MRS and ERT surveys and inversion, including 3D characterisation of clay mineralogy through alternative geophysical methods such as IP; (2) resolution and computation of fracture networks and fracture flow; (3) application of transient, variably saturated model for better accounting of mixing and processes in the unsaturated zone; (4) more research on the relationship between geophysical (ERT and MRS) porosity and hydrogeological porosity.

Acknowledgements

We acknowledge the valuable assistance provided by Harold Cole in Gortinlieve for access to his properties, practical and technical help as well as the MSc students at QUB for data collection and processing. This work is based on a research grant aided by the Irish Department of Communications, Energy and Natural Resources under the National Geoscience Programme 2007–2013 and the Geological Survey of Ireland Geoscience Research Programme 2015-2016. MRS works benefited from complementary support by the French Research Council (ANR): project Labex OSUG@2020 (ANR-10-LABX-56) and project EQUIPEX CRITEX (ANR-11-EQPX-0011) for providing the MRS equipment. The views expressed are the authors' own and do not necessarily reflect the views and opinions of the Minister for Communications, Energy and Natural Resources. Comments by two anonymous reviewers and corresponding editor Alan MacDonald are greatly appreciated and helped improving the final manuscript.

References

Ameli, A.A., Amvrosiadi, N., Grabs, T., Laudon, H., Creed, I.F., McDonnell, J.J. & Bishop, K. 2016. Hillslope permeability architecture controls on subsurface transit time distribution and flow paths, *Journal of Hydrology*, **543**, 17–30, https://doi.org/10.1016/j.jhydrol.2016.04.071

Archie, G.E. 1942. The electrical resistivity log as an aid in determining some reservoir characteristics, *Transactions of the AIME*, **146**(01), 54–62, https://doi.org/10.2118/942054-G

Ball, L.B., Caine, J.S. & Ge, S. 2014. Controls on groundwater flow in a semiarid folded and faulted intermountain basin, *Water Resources Research*, **50**(8), 6788–6809, http://dx.doi.org/10.1002/2013WR014451

Baltassat, J.M., Legchenko, A., Ambroise, B., Mathieu, F., Lachassagne, P., Wyns, R., Mercier, J.L. & Schott, J.J. 2005. Magnetic resonance sounding (MRS) and resistivity characterisation of a mountain hard rock aquifer: the Ringelbach Catchment, Vosges Massif, France, *Near Surface Geophysics*, **3**(4), 267–274

Banks, E.W., Simmons, C.T., Love, A.J., Cranswick, R., Werner, A.D., Bestland, E.A., Wood, M. & Wilson, T. 2009. Fractured bedrock and saprolite hydrogeologic controls on groundwater/surface-water interaction: a conceptual model (Australia), *Hydrogeology Journal*, **17**(8), 1969–1989, https://doi.org/10.1007/s10040-009-0490-7

Boucher, M., Favreau, G., Vouillamoz, J.M., Nazoumou, Y. & Legchenko, A. 2009. Estimating specific yield and transmissivity with magnetic resonance sounding in an unconfined sandstone aquifer (Niger), *Hydrogeology Journal*, **17**(7), 1805–1815, https://doi.org/10.1007/s10040-009-0447-x

Cai, Z. & Ofterdinger, U. 2016. Analysis of groundwater-level response to rainfall and estimation of annual recharge in fractured hard rock aquifers, NW Ireland, *Journal of Hydrology*, **535**, 71–84, https://doi.org/10.1016/j.jhydrol.2016.01.066

Carroll, D. 1959. Ion exchange in clays and other minerals, *Geological Society of America Bulletin*, **70**(6), 749–779, https://doi.org/10.1130/0016-7606(1959)70[749:IEICAO]2.0.CO;2

Cassidy, R., Comte, J.C., Nitsche, J., Wilson, C., Flynn, R. & Ofterdinger, U. 2014. Combining multi-scale geophysical techniques for robust hydro-structural characterisation in catchments underlain by hard rock in post-glacial regions, *Journal of hydrology*, **517**, 715–731, https://doi.org/10.1016/j.jhydrol.2014.06.004

Caulfield, J., Chelliah, M., Comte, J.C., Cassidy, R. & Flynn, R. 2014. Integrating petrography, mineralogy and hydrochemistry to constrain the influence and distribution of groundwater contributions to baseflow in poorly productive aquifers: Insights from Gortinlieve catchment, Co. Donegal, NW Ireland, *Science of the Total Environment*, **500**, 224–234, https://doi.org/10.1016/j.scitotenv.2014.08.105

Chandra, S., Dewandel, B., Dutta, S. & Ahmed, S. 2010. Geophysical model of geological discontinuities in a granitic aquifer: Analyzing small scale variability of electrical resistivity for groundwater occurrences, *Journal of Applied Geophysics*, **71**(4), 137–148, https://doi.org/10.1016/j.jappgeo.2010.06.003

795 Chew, D.M. 2009. Grampian orogeny. *In*: Holland, C.H. & Sanders, I.S. (eds) *The geology of Ireland*.
796 Dunedin, Edinburgh, 69–93.
797
798 Comte, J.C., Cassidy, R., Nitsche, J., Ofterdinger, U., Pilatova, K. & Flynn, R. 2012. The typology of Irish
799 hard-rock aquifers based on an integrated hydrogeological and geophysical approach, *Hydrogeology*
800 *Journal*, **20**(8), 1569–1588, https://doi.org/10.1007/s10040-012-0884-9
801
802 Cooper, M.R., Anderson, H., Walsh, J.J., Van Dam, C.L., Young, M.E., Earls, G. & Walker, A. 2012.
803 Palaeogene Alpine tectonics and Icelandic plume-related magmatism and deformation in Northern
804 Ireland, *Journal of the Geological Society*, **169**(1), 29–36, https://doi.org/10.1144/0016-76492010-
805 182
806
807 Crain, E.R. (eds) 2000. *Crain's petrophysical handbook*. Spectrum.
808
809 Daly, D., Deakin, J., Craig, M., Mockler, E.M., et al. 2016. Progress in Implementation of the Water
810 Framework Directive in Ireland. International Association of Hydrogeologists (IAH) (Irish Group)
811 Sustaining Ireland's Water Future: The Role of Groundwater, Tullamore, Co. Offaly, Ireland, 12-13
812 April 2016.
813
814 DCCAE 2017. Groundwater, Department of Communications, Climate Action and Environment,
815 Government of Ireland. http://www.dccae.gov.ie/en-ie/natural-resources/topics/Geological-Survey-
816 of-Ireland/groundwater/Pages/Groundwater.aspx
817
818 Day-Lewis, F.D., Slater, L.D., Robinson, J., Johnson, C.D., Terry, N. & Werkema, D. 2017. An overview
819 of geophysical technologies appropriate for characterization and monitoring at fractured-rock sites,
820 *Journal of Environmental Management*, **204**, 709–720,
821 https://doi.org/10.1016/j.jenvman.2017.04.033
822
823 De Marsily, G., Delay, F., Goncalves, J., Renard, P., Teles, V. & Violette, S. 2005. Dealing with spatial
824 heterogeneity, *Hydrogeology Journal*, **13**(1), 161–183, https://doi.org/10.1007/s10040-004-0432-3
825
826 Descloitres, M., Ruiz, L., Sekhar, M., Legchenko, A., Braun, J.J., Kumar, M. & Subramanian, S. 2008.
827 Characterization of seasonal local recharge using electrical resistivity tomography and magnetic
828 resonance sounding, *Hydrological Processes*, **22**(3), 384–394, http://dx.doi.org/10.1002/hyp.6608
829
830 Ellis, D.V. & Singer, J.M. 2007. *Well logging for earth scientists*. Dordrecht, Springer.
831
832 EPA 2006. Ireland; Water Framework Directive, Monitoring Programme prepared to meet the
833 requirements of the EU Water Framework Directive (2000/60/EC) and National Regulations
834 implementing the Water Framework Directive (S.I. No. 722 of 2003) and National Regulations
835 implementing the Nitrates Directive (S.I. No. 788 of 2005), Environmental Protection Agency, Co.
836 Wexford, Wexford, Ireland
837
838 Francés, A.P., Lubczynski, M.W., Roy, J., Santos, F.A. & Ardekani, M.R.M. 2014. Hydrogeophysics and
839 remote sensing for the design of hydrogeological conceptual models in hard rocks–Sardón
840 catchment (Spain), *Journal of Applied Geophysics*, **110**, 63–81,
841 https://doi.org/10.1016/j.jappgeo.2014.08.015
842
843 Gillespie, M.R., Kemp, S.J., Vickers, B.P., Waters, C. & Gowing, C.J. 2001. *Cation-exchange capacity*
844 *(CEC) of selected lithologies from England, Wales and Scotland*, SEPA R&D Technical Report, **P2-**
845 **222/TR**.

Hartmann, D.J. & Beaumont, E.A. 1999. *Predicting reservoir system quality and performance. Exploring for oil and gas traps*. AAPG Treatise of Petroleum Geology, Handbook of Petroleum Geology.

Healy, R.W. & Cook, P.G. 2002. Using groundwater levels to estimate recharge, *Hydrogeology journal*, **10**(1), 91–109, https://doi.org/10.1007/s10040-001-0178-0

Henn, F., Durand, C., Cerepi, A., Brosse, E. & Giuntini, J.C. 2007. DC conductivity, cationic exchange capacity, and specific surface area related to chemical composition of pore lining chlorites, *Journal of colloid and interface science*, **311**(2), 571–578, https://doi.org/10.1016/j.jcis.2007.02.062

Hertrich, M., Green, A.G., Braun, M. & Yaramanci, U. 2009. High-resolution surface NMR tomography of shallow aquifers based on multioffset measurements, *Geophysics*, **74**(6), G47–G59, https://doi.org/10.1190/1.3258342

Holbrook, W.S., Riebe, C.S., Elwaseif, M., Hayes, J.L., Basler-Reeder, K., Harry, D.L., Malazian, A., Dosseto, A., Hartsough, P.C. & Hopmans, J.W. 2014. Geophysical constraints on deep weathering and water storage potential in the Southern Sierra Critical Zone Observatory, *Earth Surface Processes and Landforms*, **39**(3), 366–380, http://dx.doi.org/10.1002/esp.3502

Jaunat, J., Huneau, F., Dupuy, A., Celle-Jeanton, H., Vergnaud-Ayraud, V., Aquilina, L., Labasque, T. & Le Coustumer, P. 2012. Hydrochemical data and groundwater dating to infer differential flowpaths through weathered profiles of a fractured aquifer, *Applied geochemistry*, **27**(10), 2053–2067, https://doi.org/10.1016/j.apgeochem.2012.06.009

Kolbe, T., Marçais, J., Thomas, Z., Abbott, B.W., de Dreuzy, J.R., Rousseau-Gueutin, P., Aquilina, L., Labasque, T. & Pinay, G. 2016. Coupling 3D groundwater modeling with CFC-based age dating to classify local groundwater circulation in an unconfined crystalline aquifer, *Journal of Hydrology*, **543**, 31–46, https://doi.org/10.1016/j.jhydrol.2016.05.020

Lapworth, D.J., MacDonald, A.M., Tijani, M.N., Darling, W.G., Gooddy, D.C., Bonsor, H.C. & Araguás-Araguás, L.J. 2013. Residence times of shallow groundwater in West Africa: implications for hydrogeology and resilience to future changes in climate, *Hydrogeology Journal*, **21**(3), 673–686, https://doi.org/10.1007/s10040-012-0925-4

Legchenko, A. (eds.) 2013. *Magnetic resonance imaging for groundwater*. John Wiley & Sons.

Legchenko, A.V. & Shushakov, O.A. 1998. Inversion of surface NMR data, *Geophysics*, **63**(1), 75–84, https://doi.org/10.1190/1.1444329

Legchenko, A., Comte, J.C., Ofterdinger, U., Vouillamoz, J.M., Lawson, F.M.A. & Walsh, J. 2017. Joint use of singular value decomposition and Monte-Carlo simulation for estimating uncertainty in surface NMR inversion, *Journal of Applied Geophysics*, **144**, 28–36, https://doi.org/10.1016/j.jappgeo.2017.06.010

Legchenko, A., Descloitres, M., Vincent, C., Guyard, H., Garambois, S., Chalikakis, K. & Ezersky, M. 2011. Three-dimensional magnetic resonance imaging for groundwater, *New Journal of Physics*, **13**(2), 025022, https://doi.org/10.1088/1367-2630/13/2/025022

Legg, I.C., Pyne, J.F., Nolan, C., McCardle, P., Flegg, A.M & O'Connor, P.J. 1985. *Mineral localities in the Dalradian and associated igneous rocks of county Donegal, Republic of Ireland, and of Northern Ireland*. Geological Survey of Ireland report series **RS 85/3**.

Long C.B., MacDermot C.V., Morris J.H. *et al*. 1992. *Geology of North Mayo*. GSI 1:100,000 bedrock Series, Sheet 6 map and report, GSI, Dublin

Lubczynski, M. & Roy, J. 2004. Magnetic resonance sounding: New method for ground water assessment, *Groundwater*, **42**(2), 291–309, http://dx.doi.org/10.1111/j.1745-6584.2004.tb02675.x

McConnell B.J. & Long C.B. 1997. *Geology of North Donegal: a geological description to accompany the Bedrock Geology 1:100,000 Scale Map Series*. Sheet 1 and part of Sheet 2, North Donegal, GSI, Dublin

Moe H., Craig M. & Daly D. 2010. *Poorly productive aquifers: monitoring installations and conceptual understanding*. CDM and the Environmental Protection Agency, Dublin.

Nitsche, J. 2014. *Physical characterisation of groundwater flow systems of selected poorly productive bedrock aquifers in Ireland*. PhD thesis, Queen's University Belfast, 248 p. + appendixes.

Neuman, S.P. 2005. Trends, prospects and challenges in quantifying flow and transport through fractured rocks, *Hydrogeology Journal*, **13**(1), 124–147, https://doi.org/10.1007/s10040-004-0397-2

Pilatova, K. 2013. *Characterisation of Irish poorly productive aquifers using chemical and isotopic tools*. PhD thesis, Queen's University Belfast, 332 p.

Rayner, S.F., Bentley, L.R. & Allen, D.M., 2007. Constraining aquifer architecture with electrical resistivity imaging in a fractured hydrogeological setting, *Journal of Environmental & Engineering Geophysics*, **12**(4), 323–335, https://doi.org/10.2113/JEEG12.4.323

Revil, A., Cathles, L.M., Losh, S. & Nunn, J.A. 1998. Electrical conductivity in shaly sands with geophysical applications, *Journal of Geophysical Research: Solid Earth*, **103**(B10), 23925–23936, http://dx.doi.org/10.1029/98JB02125

Ridge, M.J. 1983. A Combustion Method For Measuring The Cation Exchange Capacity Of Clay Materials, *The Log Analyst*, **24**(03).

Robins, N.S. & Smedley, P.L. 1994. Hydrogeology and hydrogeochemistry of a small, hard-rock island—the heavily stressed aquifer of Jersey, *Journal of Hydrology*, **163**(3-4), 249–269, https://doi.org/10.1016/0022-1694(94)90143-0

Schulze-Makuch, D. 2005. Longitudinal dispersivity data and implications for scaling behaviour, *Groundwater*, **43**(3), 443–456, http://dx.doi.org/10.1111/j.1745-6584.2005.0051.x

Sharp, J.M. (eds.) 2014. *Fractured Rock Hydrogeology*. CRC Press.

Singh, A. 2014. Groundwater resources management through the applications of simulation modeling: a review, *Science of the Total Environment*, **499**, 414–423, https://doi.org/10.1016/j.scitotenv.2014.05.048

Singhal, B.B.S. & Gupta, R.P. (eds) 2010. *Applied hydrogeology of fractured rocks*. Springer Science & Business Media.

Skinner, D. & Heinson, G. 2004. A comparison of electrical and electromagnetic methods for the detection of hydraulic pathways in a fractured rock aquifer, Clare Valley, South Australia, *Hydrogeology Journal*, **12**(5), 576–590, https://doi.org/10.1007/s10040-004-0356-y

Smith R.A. 1991. *Newtownards: memoir for sheet N37 and part of N38*. Geological map 1:50000 scale, British Geological Survey, Keyworth, UK

Swineford, A. 1955. *Petrography of Upper Permian Rock in South-central Kansas*. University of Kansas.

Thomas, E.C. 1976. The determination of Qv from membrane potential measurements on shaly sands, *Journal of Petroleum Technology*, **28**(09), 1087–1096, https://doi.org/10.2118/5505-PA

UKTAG 2011. UK Technical Advisory Group on the Water Framework Directive, Defining & Reporting on Groundwater Bodies, Working Paper Version V6.21/Mar/2011

Vouillamoz, J.M., Sokheng, S., Bruyere, O., Caron, D. & Arnout, L. 2012. Towards a better estimate of storage properties of aquifer with magnetic resonance sounding, *Journal of hydrology*, **458**, 51–58, https://doi.org/10.1016/j.jhydrol.2012.06.044

Vouillamoz, J.M., Lawson, F.M.A., Yalo, N. & Descloitres, M. 2014. The use of magnetic resonance sounding for quantifying specific yield and transmissivity in hard rock aquifers: The example of Benin, *Journal of Applied Geophysics*, **107**, 16–24, https://doi.org/10.1016/j.jappgeo.2014.05.012

Waxman, M.H. & Smits, L.J.M. 1968. Electrical conductivities in oil-bearing shaly sands, *Society of Petroleum Engineers Journal*, **8**(02), 107–122, https://doi.org/10.2118/1863-A

Welch, L.A. & Allen, D.M. 2014. Hydraulic conductivity characteristics in mountains and implications for conceptualizing bedrock groundwater flow, *Hydrogeology Journal*, **22**(5), 1003–1026, https://doi.org/10.1007/s10040-014-1121-5

Wiklander, L. 1964. Cation and anion exchange phenomena, *Chemistry of the Soil*, **126**, 107–148

Worthington R. & Walsh J.J. 2011. Structure of Lower Carboniferous basins of NW Ireland, and its implications for structural inheritance and Cenozoic faulting, *Journal of Structural Geology*, **33**, 1285–1299, https://doi.org/10.1016/j.jsg.2011.05.001

Zhou, Q., Liu, H.H., Molz, F.J., Zhang, Y. & Bodvarsson, G.S. 2007. Field-scale effective matrix diffusion coefficient for fractured rock: Results from literature survey, *Journal of contaminant hydrology*, **93**(1), 161–187, https://doi.org/10.1016/j.jconhyd.2007.02.002

Tables and captions

Table 1. *Summary and source of Waxman and Smits model parameters used to derive porosity values for the different aquifer units*

	Bulk resistivity* [ohm.m]	Water temperature† [°C]	Water electrical conductivity† [S/m]	Cementation factor‡ [unitless]	Cation exchange capacity§ [meq/100g]
Overburden	< 500	12.1 – 16.0	0.027 – 0.045	2.5	2.0 – 6.0¶
Broken zone	500 – 2500	12.1 – 16.0	0.027 – 0.045	2.5	2.0 – 6.0
Fissured zone	300 – 1000	12.8 – 14.2	0.029 – 0.050	2	5.2 – 18.7
Massive zone	1000 – 10 000	12.7 – 13.1	0.033 – 0.057	1.5	1.2 – 1.7

* 2D distribution obtained from ERT (see Results section).
† average values (summer 2009) recorded in boreholes (low temporal variability).
‡ from Hartmann and Beaumont (1999).
§ values calculated from mineralogical analysis and natural gamma log (see Results section).
¶ same values as for the broken zone due to lack of in situ data.

Table 2. *Clay compositions in the different boreholes and resulting bedrock clay weight fraction and cation exchange capacity (CEC)*

	Muscovite* % vs tot. clay	Chlorite* % vs tot. clay	Illite* % vs tot. clay	Montm.* % vs tot. clay	Nat. γ† cps	Clay weight fraction‡ %	Total CEC‡ meq/100g
GO1							
Broken zone (transition)	58	27	7	8	116	51	6.0
Fissured zone (shallow)	40	20	22	18	111	51	**11.7**
Massive zone (deep)	66	34	0	0	102	43	1.7
GO2							
Broken zone (transition)	75	11	8	5	101	40	3.2
Fissured zone (shallow)	18	3	47	32	102	48	**18.7**
Massive zone (deep)	82	18	0	0	116	47	1.2
GO3							
Broken zone (transition)	77	14	5	4	78	30	2.0
Fissured zone (shallow)	28	5	40	27	41	16	**5.2**
Massive zone (deep)	82	18	0	0	116	47	1.2

* dominant clay minerals that affects natural gamma logging and rock bulk CEC. CEC (muscovite)~1 meq/g; CEC (illite)~10 meq/g; CEC (illite)~20 meq/g; CEC (montmorillonite)~90 meq/g (multiple sources, see Methods section).
†average natural gamma count per seconds from borehole logging.
‡ Clay weight fraction and CEC calculated from individual clay CEC and natural gamma according to Revil *et al*. (1998).

1001 **Table 3**. *Summary of isotropic hydraulic conductivities obtained from pumping and recovery test*
1002 *interpretation and comparison with previous results*

Hydrogeological unit	Thickness from ERT [m]	Mean *K* [m/d]	*K* range [m/d]	Mean *K* from previous works* [m/d]	*K* range from previous works* [m/d]
Overburden	10 (in valley floor)	8.7	-	9	-
Broken bedrock (transition z.)	15-60	1.3×10^{-1}	$1\times10^{-1} – 2\times10^{-1}$	1	$7\times10^{-2} – 7$
Fissured bedrock (shallow z.)	5-40	1.0×10^{-2}	$3\times10^{-3} – 4\times10^{-2}$	$1\ 10^{-2}$	$1\times10^{-3} – 4\times10^{-2}$
Massive bedrock (deep z.)	>40	6.0×10^{-3}	$4\times10^{-3} – 8\times10^{-3}$	$1\ 10^{-2}$	$7\times10^{-3} – 6\times10^{-2}$

* initial hydraulic testing after drilling (Moe et al. 2010) using Horslev (infiltration tests) and Theis-Jacob (pumping tests)

1003
1004
1005 **Table 4**. *Recharge values recalculated using the water table fluctuation methods and the specific*
1006 *yield values derived from MRS. Borehole name suffixes SS (subsoil), T (transition) are derived from*
1007 *the codes listed in section Hydrogeological setting*

	Rainfall* [mm/y]	Water table cumulated rise* [m]	Specific yield† [%]	Calculated recharge [mm/y]	Calculated recharge [% of rainfall]
Hillslope					
GO1T 2010-2011	1134	13.6	0.75	102	9
GO1T 2011-2012	1433	19.7	0.75	147	11
GO2T 2010-2011	1134	8.8	1.57	138	13
GO2T 2011-2012	1433	16.8	1.57	264	19
Average				163	13
Valley floor					
GO3SS 2010-2011	1134	7.4	3	222	21
GO3SS 2011-2012	1433	11.7	3	351	24
Average				287	23

* from Cai & Ofterdinger (2016)
† from MRS, assuming specific yield = 0.5*MRS water content

1008
1009
1010 **Table 5**. *Details of key hydrogeological parameters and recharge values applied to Model 1 and 2*

	*Kmax** [m/d]	*Kmin*/*Kmax* [unitless]	Anisotropy angle [°]	Porosity† [%]	Recharge‡ [mm/y]
Model 1					
Overburden	9	1	Isotropic	20	Valley floor: 95 (480)§
Broken zone	1 (0.2)§	1	Isotropic	4	Hillslope: 75 (370)§
Fissured zone	0.01 (0.002)§	1	Isotropic	0.2	NA
Massive zone	0.01 (0.002)§	1	Isotropic	0.01	NA
Model 2					
Overburden	8.6	1	Isotropic	7	Valley floor: 285
Broken zone	0.14	0.5	75 ° dip NW	3	Hillslope: 165
Fissured zone	0.014	0.3	85 ° dip SE	0.1-0.5	NA
Massive zone	0.008	0.1	65 ° dip SE	0.01	NA

* from Moe *et al*. (2010) for Model 1; from Comte *et al*. (2012) for Model 2
† from Comte *et al*. (2012) for Model 1; from Waxman and Smits' model and MRS results for Model 2 (Figure 7)
‡ from Cai & Ofterdinger (2016) for Models 1; recalculated values for Model 2 (Table 4)
§ values in brackets are final values after model calibration to observed heads in boreholes (*K*/5 and Recharge*5)

Figure captions

Fig. 1. *Study site physical setting maps; (**a**) site location within the Irish basement geological framework (modified from Geological Survey of Ireland 2006); (**b**) catchment boundary with location of hydrological monitoring infrastructures; (**c**) local interpretative geological map with location of the borehole clusters, the ERT profile and the MRS soundings.(**a**) and (**b**) modified from Comte* et al*. (2012).*

Fig. 2. *Generic hydrogeological conceptual model of weathered/fractured rocks aquifers in the context of the Irish terminology (modified from Comte* et al*. 2012).*

Fig. 3. *Fracture pole density distributions (Schmidt net lower hemisphere projection) and orientations (fracture azimuth rose diagrams) from outcrops and boreholes (acoustic televiewer probe); blue points and arrows show the hydraulically active fractures unambiguously identified in boreholes (Nitsche 2014; modified from Comte* et al*. 2012)*.

Fig. 4. ERT results (**a**) and interpreted conceptual model of the weathered/fractured aquifer (**b**).

Fig. 5. *Comparison of hydraulic conductivities obtained from; (**a**) initial isotropic hydraulic test interpretations from Moe* et al*. (2010) used in Model 1; (**b**) refined isotropic interpretation from Comte* et al*. (2012); and (**c-e**) anisotropic* K *values used in Model 2, (**c**)* K_{max}*, (**d**)* $K_{equivalent}$*, and (**e**)* K_{min}*.*

Fig. 6. *Vertical distribution of MRS water content for the 8 MRS sounding (see locations on Figure 1) and comparison with the aquifer conceptual model units delineated from ERT (Figure 4)*.

Fig. 7. *Spatial variations of storage properties derived from ERT and MRS geophysical data; (**a**) ERT resistivity model with location of approximate volume of investigation of the MRS soundings; (**b**) MRS water content logs; (**c**) ERT porosity calculated from Waxman & Smits' model. Hatched areas indicate the unsaturated zone for which saturated Archie and Waxman & Smits models used are not applicable.*

Fig. 8. *Conceptual aquifer geometries implemented in the numerical models: (**a**) generic tabular structure of weathered/fractured layers from borehole interpretation (Model 1); (**b**) complex layered structure derived from geophysical data reconciled with borehole logs (Model 2). 1: Overburden (alluvial and glacial sediments); 2: Broken bedrock (transition zone); 3: Fissured (shallow) bedrock; 4: Massive (deep) bedrock; 5: Substratum (very low productivity).*

Fig. 9. *Simulation results for Model 1 (**a,b,c**) and Model 2 (**d,e,f**) showing groundwater seepage rates at the model surface, Darcy's fluxes variations across the transect (**a,d**), groundwater mean flowpaths (**b,e**), and groundwater ages (**c,f**).*

Fig. 10. *Relative distributions of groundwater flow rate (as % of total flow) in the four conceptual aquifer units (overburden, broken, fissured and massive bedrock) for the two models considered. The massive bedrock here also includes the deeper levels shown in Figure 8.*

Fig. 11. *Modelled groundwater ages in the different boreholes for the two model cases. The hatched area indicates groundwater ages that are older than the modern period of high atmospheric Tritium levels, and inconsistent with measured Tritium concentrations in boreholes samples.*

Catchment-scale heterogeneity of flow and storage properties in a weathered/fractured hard rock aquifer from resistivity and magnetic resonance surveys: Implications for groundwater flow paths and residence times distributions

J-C. Comte[1,*], U. Ofterdinger[2], A. Legchenko[3], J. Caulfield[4], R. Cassidy[5], J. A. Mézquita González[1]

[1]University of Aberdeen, School of Geosciences, Aberdeen AB24 3UF, UK
[2]Queen's University Belfast, School of Natural and Built Environment, Belfast BT9 5AG, UK
[3]IRD/Université Joseph Fourier, Grenoble, France
[4]Trinity College Dublin, School of Natural Sciences, Department of Geology, Dublin 2, Ireland
[5]Agri-Food and Biosciences Institute (AFBI), Belfast BT9 5PX, UK
*Correspondence (jc.comte@abdn.ac.uk)

Running Title

Flow and storage properties of fractured rocks

Abstract

Groundwater pathways and residence times are controlled by aquifer flow and storage properties, which are characterised by high spatial heterogeneity in weathered/fractured hard rock aquifers. Building on earlier work in a metamorphic aquifer in NW Ireland, new clay mineralogy and geophysical data analyses provided high spatial resolution constraints on the variations of aquifer properties. Groundwater storage values derived from magnetic resonance sounding and electrical resistivity tomography were found to largely vary laterally and with depth, by orders of magnitude. Subsequent implementation of numerical, 2D-hillslope groundwater models showed that incorporating heterogeneity from geophysical data in model parametrisation led to best fit to observations as compared to a reference model based on borehole data only. Model simulations further revealed that; 1/strong spatial heterogeneity produces deeper, longer groundwater flow paths and higher age mixing in agreement with the mixed sub-modern/modern ages (mostly <50 years) provided by independent tritium data; 2/areas with extensive weathering/fracturing are correlated with seepage zones of older groundwater, due to changes in the flow directions, and are likely to act as drainage structures for younger groundwater on a catchment or regional scale. Implications for groundwater resilience to climate extremes and surface pollution are discussed along with recommendations for further research.

Weathered/fractured hard rock aquifers underlie over 20% of the global land surface (Sharp 2014) and are characterised by a high degree of structural heterogeneity and overall low productivity. In recent years, water managers and policy-makers have moved to adopt a catchment scale approach to the integrated management of surface and subsurface water resources (EU Water Framework Directive 2000/60/EC), including the UK (UKTAG 2011) and Ireland (Daly *et al*. 2016). Understanding spatial variations of aquifer hydraulic properties at the catchment-scale, which dictates groundwater flow pathways and residence times, is crucial to inform catchment management plans. Yet, resolving such spatial heterogeneity in fractured bedrock remains very challenging due to the typically scattered nature of direct observations points (boreholes and outcrops) that usually do not have sufficient spatial coverage to capture the scale of heterogeneity (De Marsily *et al*. 2005; Neuman 2005).

To address the lack of spatial resolution in heterogeneous fractured rock catchments, traditional direct testing techniques in boreholes, such as hydraulic testing and geophysical logging, are increasingly combined with indirect and more spatially integrative investigation methods, including tracer testing (e.g. Klepikova 2016), geophysical imaging (ground- or airborne-based) (Comte *et al*. 2012; Shakas *et al*. 2016; Day-Lewis *et al*. 2017) and remote sensing (Cassidy *et al*. 2014; Frances *et al*. 2014). The use of geophysics has long proven effective in resolving, at catchment scale, the heterogeneity of fractured rock aquifers (Holbrook *et al*. 2014; Robinson *et al*. 2016). The Electrical Resistivity Tomography (ERT) method is known to be efficient at imaging spatial variability in weathering, geological heterogeneity and fracture patterns (e.g. Chandra *et al.* 2010; Rainer *et al*. 2007). All ERT studies, however, stress the importance of *a priori* information, especially borehole data and outcrop mapping to support its hydrogeological interpretation (Skinner & Heinson 2004; Comte *et al.* 2012).

A number of studies have demonstrated the benefits of using ERT in combination with other geophysical methods; in particularly with the magnetic resonance sounding (MRS) that complements imaging of heterogeneity by ERT with lower resolution but more quantitative information on water storage. Both methods have, for instance, been used to map groundwater occurrence and develop hydrogeological conceptual and numerical models in weathered basement aquifers (Frances *et al.* 2014; Baltassat *et al.* 2005) and monitor groundwater recharge (Descloitres *et al.* 2008). As yet, however, most of these studies have focused on low latitude regions with deep and relatively water-productive weathering horizons (saprolite) that produce strong MRS and ERT responses for relatively simple, layered aquifer geometries. There are fewer examples in higher latitude catchments with a glacial legacy, such as in Ireland, where most of the saprolite (relatively high storage, porous layer) is absent, exposing only the fractured (low storage) and structurally complex bedrock. In addition, these geophysical approaches still remain either (i) not systematically applied in catchment groundwater studies or (ii) applied qualitatively, i.e. used to inform aquifer heterogeneity conceptual models rather than to quantify spatial variations in aquifer properties (permeability and porosity). This needs further consideration in highly heterogeneous basement rock catchments.

In Ireland, the fractured rock aquifers provide a good analogue of temperate region bedrock aquifers with a glacial legacy. The island of Ireland is underlain by over 60**%** of hydrogeologically poorly-productive fractured bedrock (Moe *et al.* 2010), either cropping out directly or covered by superficial glacio-fluvial and/or alluvial sediments. Most of this poorly-productive bedrock is composed of various grades of metamorphic (basement) rocks; from low-grade metasediments to high-grade gneiss-migmatites and granitoids. Groundwater in these rocks, despite their overall low productivity, is nonetheless crucial for maintaining river base flow during dry periods and supporting aquatic ecosystems and small-scale rural water supply (DCCAE 2017). Over the last decade, the extension of the Irish national groundwater monitoring network to poorly productive basement aquifers as part of implementing the European Union's Water Framework Directive (EPA 2006; Moe *et al.* 2010) has stimulated hydrogeological research through Irish Government-funded projects. Among them, the Griffith Poorly-productive Aquifers Project (2007-2014), on which this work is based, aimed to improve the understanding of groundwater flow regimes in fractured rock aquifers

and the contribution of groundwater to catchment water balance (Comte *et al.* 2012; Cassidy *et al.* 2014; Caulfield *et al.* 2014; Cai & Ofterdinger 2016).

This paper presents an overview of the latest research in a micaschist catchment in Co. Donegal, Republic of Ireland, with the aim of resolving catchment-scale spatial variations of aquifer properties. It synthesises previously published research on aquifer typology and well-scale hydraulics (Comte *et al.* 2012; Cassidy *et al.* 2014), bedrock weathering (Caulfield *et al.* 2014) and aquifer storage properties (Legchenko *et al.* 2017), augmented with the latest results from quantitative interpretation of geophysical data (ERT and MRS) to provide a robust spatial understanding of flow and storage property fields. This work further explores the integration of the existing knowledge on the heterogeneity of aquifer properties using numerical models to assess groundwater flow paths and residence time distributions. Finally, we use the results to discuss the impact of climate change and contaminant transport on groundwater resources and catchment management, as well as further recommendations for improved groundwater modelling.

Hydrogeological setting

Geology

The Gortinlieve catchment (5 km^2), Co. Donegal, NW Ireland (Figure 1) is underlain by Late Precambrian micaschists and psammites of intermediate metamorphic grade (low amphibolite facies). These belong to the Grampian terrane in Co. Donegal as part of the Southern Highland Group, spanning through Ireland and Scotland. They originate from turbidite sequences deposited c. 550 Ma BP (McConnell & Long 1997; Caulfield *et al.* 2014) and subsequently subjected to poly-phase deformation and metamorphism during the Caledonian orogeny. The Caledonian tectonic regime associated with the closure of the Iapetus Ocean (Grampian phase, early Ordovician) generated the current regional NE–SW oriented structures (Chew 2009) characterised by fault scarps and cartographic/topographic lineaments visible in the upper catchment (Fig. 1). The later Taconic phase (late Ordovician) generated the current WNW-ESE orientation deformational structures and imprinted the retrograde amphibolite metamorphic facies (McConnell & Long 1997). The current, Alpine, strike-slip tectonic regime, is reflected by reactivation of NE-SW fracture orientations and further creation of a general NW-SE trend (Worthington & Walsh 2011; Cooper *et al.* 2012). Localised kaolinite rich Tertiary lateritic horizons preserved on Grampian rocks of western Ireland (Legg *et al.* 1985) provide evidence that the basement was during this time at least partially exhumed and undergoing tropical weathering. Subsequent Quaternary glaciations have resulted in further erosion, including the removal of the upper levels of the weathering profiles, most pronounced in high topographic areas, and in the deposition of heterogeneous glacio-fluvial material (clay-till and sand and gravel) in low-lying areas and valley bottoms.

Hydrogeology and borehole instrumentation

Annual rainfall in the area ranges from 1000 to 1200 mm and mean temperature annually ranges from 6 to 14 °C (Met Eireann 2017). The catchment comprises a headwater stream network of a Carrigans River, a tributary of the River Foyle that discharges into the Atlantic Ocean, approx. 40 km NE of the catchment (Caulfield *et al.* 2014). The Gortinlieve catchment was instrumented with monitoring boreholes by the Irish Environmental Protection Agency (EPA) in 2006 as part of the national groundwater monitoring programme. Three borehole clusters were sited in a linear hillslope transect at high (GO1, 174 m above mean sea level; hereafter noted m amsl), intermediate (GO2, 88 m amsl) and low (GO3, 33 m amsl) elevations within the catchment. Individual clusters contain up to 4 boreholes, each isolated and screened across different depth-distinctive zones commonly encountered in Irish bedrock aquifers. The initial classification of Moe *et al.* (2010)

conceptually described these respective intervals as; subsoil SS (average interval 1–3 m below ground surface (bgs); only present in Gortinlieve at the valley bottom), transition zone T (average interval 4–5 m bgs), shallow bedrock S (average interval 8–19 m bgs) and deep bedrock D (average interval 30–67 m bgs). The conceptual model was further refined by Comte *et al.* (2012) in order to help reconcile geological features with geophysical constraints (Fig. 2): overburden deposits (cf. subsoil); broken bedrock (cf. transition zone); fissured bedrock (cf. shallow bedrock); massive bedrock (cf. deep bedrock). The Irish EPA monitors water levels at 15-minute intervals in each borehole using automatic data loggers. The site was also equipped with an automated tipping bucket rain gauge (AEG 100) since October 2010 for the duration of the project.

Aquifer characterisation methods

Structural, mineralogical and hydraulic investigations

Detailed analysis of fracture patterns and clay occurrence in the bedrock was carried out in order to establish the micro- to meso-scale structural controls on groundwater flow, and to provide constraints on larger (meso- to macro) scale hydraulic and geophysical interpretations and numerical modelling.

Fracture orientations were measured on maps, outcrops, boreholes and quarry exposures. Regional structural trends were determined from interpretation of the geological map (Smith 1991; Long et al. 1992; McConnell & Long 1997) and the 20-m resolution digital elevation model (Ordnance Survey of Ireland). During field mapping, the main fracture parameters measured were strike, dip magnitude, dip azimuth with a minimum of 30 fracture measurements for each sample site, subsequently plotted as rose diagram and Schmidt net pole density distribution. The acquisition and plotting methodology are described in details in Comte *et al.* (2012) and Nitsche (2014). Borehole fractures were analysed using acoustic televiewer logs. Among these, hydraulically active fractures were identified through cross-correlation with electrical conductivity logs whereby marked changes in water electrical conductivity at the depth of observed fractures was interpreted as fracture flow (Nitsche 2014).

Mineralogical and petrographic data are summarised by Caulfield *et al.* (2014). Representative field outcrop and recovered borehole core samples were further characterised in this study to quantify the relative proportions of identified phyllosilicate minerals to assess their influence on geoelectrical properties. The mineral modes of the dominant basement lithologies (psammitic schists uphill vs. micaschists downhill) were quantified by petrographic point-counting (500 points per slide). These compositions were taken to represent fresh, primary (unweathered) bedrock. Free phyllosilicate minerals (mineral grains not bound in the competent fresh bedrock structure) were separated and collected from weathered samples by repeated washing with distilled water and dried at 50°C. Clay sized (<2 µm) fractions were obtained following the method outlined in Caulfield *et al.* (2014), and references therein. The relative proportions of primary (muscovite, chlorite) and secondary (illite, montmorillonite and illite/montmorillonite admixtures) were determined via thermogravimetric analysis (TGA) using a Netzsch libra thermogravimetric analyser, in conjunction with XRD and FTIR results from Caulfield *et al.* (2014). Samples were heated from 200-880°C to determine sequential dehydroxylation water loss from the clay mineral fraction. Mineral proportions (volume %) were converted to weight %. Using the method of Revil *et al.* (1998), the total cation exchange capacity (CEC) of the different geological units (transition, shallow, deep bedrock) at each of the three sites (GO1-3) were calculated from (i) the relative mass proportion of clay minerals, (ii) their individual CEC, obtained from literature (Swineford 1955; Carroll 1959; Wiklander 1964; Thomas 1976; Ridge 1983; Revil *et al.* 1998; Crain 2000; Gillespie *et al.* 2001; Ellis & Singer 2007; Henn *et al.* 2007) and (iii) the total clay content derived from natural gamma ray logs from each borehole.

Aquifer pumping and recovery tests were implemented in every borehole to provide local values of equivalent hydraulic conductivity and storativity for each borehole. The hydraulic testing methodology is described in details in Comte *et al.* (2012). Pumping test were conducted at a constant rate (2 to 30 L/min depending on the borehole) and both pumping and recovery curves were jointly interpreted using AQTESOLV Pro v4.5 and applying a range of adapted analytical solutions (with regards to the known aquifer structure and the borehole technical characteristics) including single porosity/permeability models. Hydraulic conductivities (*K*) were calculated from transmissivity values using observed unit aquifer thicknesses from borehole data, ERT data and geophysical logging data.

K in fractured rocks is typically anisotropic, i.e. directionally dependent implying different *K* values in different directions, with the maximum hydraulic conductivity *Kmax* following the direction of the hydraulic active fractures and the minimum hydraulic conductivity *Kmin* being orthogonal to the hydraulic active fractures. This further implies that the anisotropy angle in fractured rocks, because of the presence of steep fractures, has a higher vertical component than in most sedimentary rocks where the direction of *Kmax* is often sub-horizontal, parallel to the sedimentary bedding (in this case *Kmax* is usually denoted *Kh*) and the direction *Kmin* is subvertical (and in this case denoted *Kv*). In this work, values of hydraulic conductivities provided by hydraulic tests were further analysed in terms of anisotropy in 2D (along the studied transect). As hydraulic test values were assumed equivalent to isotropic hydraulic conductivities, the integration of fracture analysis data allowed for the definition of *Kmax* *Kmin* and anisotropy angles (by definition the angle of *Kmax* to the horizontal) based on the measured orientation of the hydraulically active fractures. The anisotropy ratio *Kmin*/*Kmax* (unitless) was derived by considering it to decrease with depth from 0.5 to 0.1. At depth, where the steep fracture sets dominated (see section *Aquifer characterisation results*) and produced a stronger anisotropy, the ratio was set to 0.1, whereas at shallow depths, where other fracture sets and pronounced weathering contribute to flow, particularly in the broken bedrock, anisotropy was expected to weaken and was therefore set to 0.5. The anisotropy angle was derived as an average of the individual angles of the dominant fracture sets for each bedrock conceptual unit (broken, figured, massive).

Geophysical investigations

Electrical resistivity tomography and petrophysical models for porosity estimation

A geophysical survey using electrical resistivity tomography ERT was carried out to provide a catchment-scale conceptual understanding of the bedrock heterogeneity and its hydrogeological significance. ERT was applied along the hillslope transect of the three well clusters using a Syscal Pro 72 resistivity meter. As described in Comte *et al.* (2012), the acquisition was carried out with 60 electrodes at 5-m unit electrode spacing, subsequently expanded through roll-along. The dipole-dipole (DD) and multi-gradient (mGD) quadripole configurations ran sequentially, ultimately allowing a depth of investigation of 50–60 m (Edwards 1977). After noise removal, DD and mGD apparent resistivity data were jointly inverted using RES2DINV v3.58. The inversion provided a 2D model of specific resistivities in which model regions that are insensitive to the input data were removed using the depth of investigation (DOI) method of Oldenburg & Li (1999). The best model retained for hydrogeological interpretation was obtained for the 5th iteration, giving an absolute error between observed and calculated apparent resistivities of 9.6%.

In addition to the structural information provided by the interpretation of spatial resistivity variation, a petrophysical model was applied to the resistivity model in order to derive bedrock porosity. Due to the substantial amount of clay minerals (both primary and secondary) in the psammites and the micaschists, Archie's model (Archie 1942) was not applicable and instead, the Waxman and Smits (1976) model was used. The Waxman and Smits model relates the bulk (specific) resistivity obtained by inversion to the aquifer total porosity (which is the unknown to resolve), the

pore water saturation (equal to one below the water table), the rock matrix cementation factor, the groundwater electrical conductivity and temperature, and in addition to Archie's Model, the total rock CEC, which was obtained from mineralogical investigations and natural gamma logs (see section *Aquifer characterisation results*). The model is described in Revil et al. (1998) and was applied to estimate the 2D (hillslope) distribution of total porosity along the transect imaged by ERT. Table 1 summarises the values of the parameters used for the different hydrogeological units.

Magnetic Resonance Sounding

The magnetic resonance sounding (MRS) method (Legchenko 2013) was applied at 11 points along the ERT transect and close to the borehole clusters (Fig. 1). The MRS surveys provided 1D (vertical) profiles of water content. MRS measurements were performed in two surveys, in 2010 and 2016 using the NUMISPLUS and NUMISPOLY instruments, respectively, both developed by IRIS Instruments (France). As described in more detail in Legchenko *et al*. (2017), figure-eight square loops were applied in three configurations: two cable turns of 25-m-side, one turn of 37.5-m-side, and one turn of 50-m-side, with a reference loop in 2016 to improve the signal to noise ratio, which is typically low in fractured rock environments, due to a low water content. Eight out of the 11 MRS soundings had acceptable signal-to-noise ratios; the remaining three are not considered in this work. 1D inversion of MRS data was carried out using the SAMOVAR software package. It used the Tikhonov regularization method (Legchenko & Shushakov 1998) and the uncertainty in the inversion results was examined applying Monte-Carlo simulations (Legchenko *et al*. 2017). Geological interpretation of MRS results was performed taking into account the thicknesses of the aquifer units (broken and fissured zone) identified with ERT as structural constraints.

Estimation of aquifer storage parametres from ERT porosity and MRS water content

ERT porosity and MRS water content were used to derive aquifer specific yield *Sy* and effective porosity n_e subsequently used for recharge estimation, and numerical groundwater modelling, respectively. By definition, n_e is the interconnected porosity controlling groundwater mass transport and residence times. Also by definition, *Sy*, also called drainage porosity, is the mobile pore water not retained by capillarity forces and controls water table fluctuations in unconfined aquifers.

In fractured rocks, where porosity is mostly the result of the opening of fractures and foliation planes by (groundwater-aided) weathering, the occurrence of closed (unconnected) pore space is limited (Singhal & Gupta 2010). This implies that total porosity, obtained from ERT, can be considered a close estimate of the effective porosity n_e, which was our assumption for subsequent modelling.

The MRS water content is commonly reported (Lubczynski & Roy 2004) as being correlated with, and representing an intermediary between, the drainage porosity *Sy* (mobile pore water non retained by capillarity forces) and the effective porosity n_e (immobile and mobile interconnected pore water). Recent studies carried out in low porosity fractured environments (Vouillamoz *et al.* 2012, 2014) have reported MRS water content values linearly correlated to, although higher than *Sy* (within a factor 2) estimated through pumping tests. Consequently, for subsequent recharge calculations we have taken *Sy* at half (0.5 times) the measured MRS water content.

Recharge estimations

Recharge values were calculated with the water table fluctuation method applicable to recharge estimation in unconfined aquifers (Healy & Cook 2002). The method requires water table time-series as well as well as values of the specific yield at depth where the water table fluctuates. We used the piezometric fluctuations in the shallowest boreholes (GO1T, GO2T and GO3SS) as reported in Cai & Ofterdinger (2016) for the period 2010-2012. For the specific yield, we used the MRS derived values

obtained at the approximated depth of the water table (see previous Section) from the MRS soundings nearest to the boreholes; MRS1 and MRS2 for GO1T, MRS4 and MRS5 for GO2T, and MRS8 for GO3SS.

Aquifer characterisation results

Aquifer structure and weathering

Fracture analysis

Measurements of hydraulically active fracture from both outcrops and boreholes at the site showed dominant meso-scale (millimetre to metre) fracture occurrences and orientations which correlate with established past tectonic regimes in Ireland (Fig. 3). Two dominant hydraulically active fracture sets were identified: a dominant set with fractures oriented E-W to NE-SW with a dip angle of about 60-80° S to SE; and a less frequent set with fractures also oriented E-W to NE-SW but with a dip angle of about 60-90° N to NW. The dominant fracture set may be attributed to the strike-slip regional fracturing associated with Alpine compression during the Palaeocene, whereas the second set may be attributed to the compressive fabric of the Neo-Proterozoic to late Carboniferous orogenies (Grampian, Caledonian and Variscan), which also characterise the regional-scale lineaments (Fig. 1) and Lower Carboniferous normal faults (Worthington & Walsh 2011), reactivated by the Alpine strike-slip regime (Cooper *et al*. 2012). The most frequently recorded fracture set is oriented WNW–ESE with a low dip angle of 35 ° NNE corresponding to the highly weathered Dalradian schistosity plane (see below). However, this set does not appear to be clearly associated with hydraulic activity in boreholes and therefore may only play a role in the uppermost levels of the aquifer (broken bedrock and possibly the upper part of the fissured bedrock) for which hydraulic activity in boreholes is difficult to record due to their shallow depths and denser weathering/pervasive fracturing.

At macro-scale (catchment and regional scale, i.e. 100 m to km; Fig. 1b), cartographic lineaments attributed to glacial erosion preferentially affecting regional geological boundaries and deep weathering corridors were found to be typically associated with the measured pre-Alpine NE–SW trend (Comte *et al*. 2012).

Mineral analysis

Mineralogical investigations reveal that phyllosilicate minerals are dominated by muscovite and chlorite (primary) and illite and montmorillonite (secondary clays produced by weathering of chlorite and muscovite) (Caulfield *et al*. 2014). Major non-clay minerals comprise quartz and feldspar.

Relative proportions of clay minerals versus the total clay mass fraction are presented in Table 2. The massive (unweathered) bedrock encountered in the deep boreholes was found to contain negligible secondary clays, with only primary chlorite and muscovite observed. The fissured zone in boreholes GO2 and GO3 contained an approx. equal mixture of illite and montmorillonite with lesser amounts of chlorite and muscovite, and in GO1, relatively even quantities of the four minerals. This suggests a moderate weathering of the fissured zone primary clays in GO1, whilst in GO2 and GO3, they have undergone major weathering as evidenced by the almost complete absence of chlorite. Over 80% of clays in the broken zone were muscovite and the remaining 20% approx. equal proportions of illite and montmorillonite. Because weathering is most active in the broken zone, it was concluded that secondary clays are transported in suspension downward from the broken zone and redeposited in the underlying fissured zone (Comte *et al*. 2012; Caulfield *et al*. 2014).

Table 2 also details the total clay mass fraction as derived from natural gamma ray logs. The relative proportions of clay minerals and the total clay mass fraction allowed calculation of the total CEC of the different aquifer units using the model of Revil *et al*. (1998). The total clay content of the

different aquifer units (broken, fissured and massive bedrock) was not significantly different; however due to significant differences in clay mineralogy, the resulting CEC is different. The fissure bedrock, with a higher proportion of illite and montmorillonite (secondary weathering clays characterised by high CECs) consistently produced the highest bulk CEC values. The massive bedrock dominated by muscovite and chlorite (primary clays characterised by low CEC values) produced the lowest bulk CEC. This CEC distribution is relevant to the interpretation of ERT results and application of the petrophysical models in which it is a key input parameter.

Geophysical structure

Results of the ERT investigations provide cross-sectional variations of electrical resistivity along the borehole hillslope transect (Figure 4), revealing a high degree of aquifer heterogeneity. As electrical resistivity is primarily controlled by porosity (fracture porosity in the present context), clay content and mineralogy, its spatial variations can be interpreted as reflecting changes in lithology, pore water saturation, open fracture density and weathering intensity. Resistivity values range from about 100 ohm.m to just under 10 000 ohm.m, i.e. three orders of magnitude. Highest resistivities (>> 1000 ohm.m) were observed at the base of the transect and reflect the massive micaschist unit beneath the weathered front, characterised by a low density closed fractures and small quantities of secondary weathering clays. Some equally high resistivity values were also obtained in the very shallow subsurface in the higher elevation part of the profile. Correlations with the depth of the water table in borehole cluster GO1 and observed spring lines at its base suggested that this uppermost, high resistivity unit corresponds to unsaturated, clay-poor psammite-schist. The lowest resistivity values (<500 ohm.m) were obtained at a relatively shallow depth in the flood plain and corresponded to the clay-till and alluvium overburden. Intermediate resistivity values (500-2500 ohm.m) were observed throughout the whole transect at shallow to intermediate depths (0 to about 50 m below surface) and characterised the heterogeneous weathered/fractured schists (broken and fissured bedrock). The relatively continuous unit with values ranging ~300-1000 ohm.m overlying the massive bedrock are interpreted as fissured bedrock characterised by a high density of open fractures possibly filled with high-CEC weathering clays as suggested by the clay mineralogy. This fissured layer was particularly deep at three locations along the transect; at the following horizontal distances from NW end of the profile of X=400-500 m, 750-850 m and 1100-1300 m. Since they correlate well with the regional Grampian lineaments (Fig. 1), these locations are interpreted as deep fractured zones that facilitate deep weathering. At these three locations a slightly more resistant layer was observed overlying the fissured layer, with resistivities in the range of 500-2500 ohm.m. This unit is interpreted as the broken schists (transition zone) where the weathered clays have been leached and transported to the underlying fissured zone.

Flow properties

Pumping and recovery tests in every borehole provided estimates of (equivalent isotropic) hydraulic conductivities *K* for bedrock and overburden (Table 3). A clear trend of decreasing hydraulic conductivity with depth is observed. The broken bedrock (transition zone) displayed mean values close to 10^{-1} m/d, the fissured bedrock close to 10^{-2} m/d with large variability of over two orders of magnitude and the massive (deep) bedrock around 6 x 10^{-3} m/d. The overburden (glacio-fluvial and alluvium deposits) present in the valley floor displayed much higher mean *K* values of ~9 m/d. These values partly agree with values from previous hydraulic tests by Moe *et al*. (2010). These authors obtained much higher mean *K* for the broken bedrock due to one very high value (of about 7 m/d) obtained in the valley floor at GO3, which may be representative of the interface between the overburden glacio-fluvial deposits and the bedrock. They also provided values for the deep massive bedrock that are similar to those in the overlying fissured (shallow) bedrock.

Kmax, *Kmin* and the anisotropy angles (angle of *Kmax* to the horizontal plane, in °) in the 2D vertical plane of the studied transect were further derived based on the measured orientation of the dominant, hydraulically active fracture sets (see previous Section); a primary set ~70° dipping SSE and secondary set ~75° dipping NNW, and another set ~35° dipping NNW which is not clearly hydraulically active at large depths, but is probably active in the weathered near-surface. The anisotropy ratio *Kmin*/*Kmax* (unitless) was assumed to decrease with depth from 0.5 to 0.1 (see Section *Methods*). The calculated anisotropy angle increased with depth from a relatively low angle in the broken bedrock as a result of the equal contribution of the three fracture sets (75° NW) to a dominant steep angle in the deep bedrock (70° SE, parallel to dominant hydraulically active Variscan-Alpine fabrics). Fig. 5 plots the values of *Kmin*, *Kmax* along with the previous equivalent isotropic *K* estimates (Moe *et al*. 2010; Comte *et al*. 2012). The values of *Kmax* were close to the values obtained from hydraulic tests, which were assumed to preferentially mobilise groundwater from the fractures responsible for *Kmax* (direction of maximum anisotropy).

Storage properties

Quantitative information on the heterogeneity of aquifer storage properties was provided by the joint analysis of hydraulic test results and geophysical data (MRS and ERT). Hydraulic test results are limited to single estimates of specific yield (*Sy*). Moreover, *Sy* values obtained from measurements in pumped wells in absence of observation wells are usually inaccurate due to possible well bore storage effects. However they did provide indicative orders of magnitude as a guide, with broken bedrock displaying *Sy* values around 3-5 %, fissured bedrock of about 0.1 % and massive bedrock around 0.001 %, i.e. over an order of magnitude decrease between each layer with increasing depth.

Geophysical data provided higher resolution spatial information on the variability of storage properties. MRS, despite an instrumental sensitivity that currently does not reliably quantify less than 1 % water content, detected appreciable quantities of water above 2% in the central and low part of the transect (Fig. 6). The highest water contents were detected at MRS8 in the valley floor with values between 2 and 6 % at shallow depths (0-25 m) corresponding to the occurrence of the relatively porous overburden materials and the broken bedrock. Similar water content values were also obtained at MRS4, upslope of GO2, at depths (2-15 m) consistent with the area of deep weathering identified by ERT (X=400-600 m on Fig. 4) and characterised by significant deepening of the broken bedrock layer. In the upper part of the transect around GO1, no appreciable water content was detected by MRS suggesting water content < 1 %. This is also the case for the two soundings carried out between GO2 and the valley floor. Overall, the MRS results show relatively good agreement with the depth delineation of the broken bedrock and overburden layers from ERT (Fig. 6 and 7a,b). For the overburden in the valley floor, MRS water content values of approx. 5-6 % were obtained while the broken bedrock (transition zone) yielded values of 2-4 %. At depth below the base of the broken layer (as delineated with ERT), MRS mostly provided either water content values below the normal limit of detection of the methods (1 % water content) or values with high inversion uncertainty. This suggests that the fissured and massive bedrock had water content values < 1 %. Note that the broken bedrock, which is likely present in the upper part of the transect was mostly unsaturated in the summer (dry) conditions when both ERT and MRS surveys were undertaken.

The Waxman and Smits model (Fig. 7c), provided spatial variations of (effective) porosities consistent with MRS results, and porosity values of about half the MRS water contents. Values ranging from 3-7 % were obtained in the overburden/broken bedrock of the valley floor while the broken layer of the mid and upper part of the transect displayed values ranging from 1 to 3 %, decreasing with distance to valley floor. For the fissured layer, we obtained values between 1 % beneath the valley floor to less than 0.1 % in the upper part of the transect, with a relatively progressive decrease from valley bottom to hilltop. Porosities lower than 0.03 % were obtained in the massive, unweathered bedrock layer. As a comparison, Archie's model (not presented here),

which is applicable in clay-free materials, provided much higher, unrealistic porosity values of about an order of magnitude (i.e. about ten times) higher, ranging 1 to 40 %. This confirmed that Archie's model is not applicable in this type of environment due to significant clay content.

The slightly lower (effective) porosities values obtained from the Waxman and Smits model as compared to the MRS water content values, of approximately a factor of two, are consistent with the findings from Vouillamoz *et al*. (2012, 2014) who reported similar difference factors in low porosity (< 3 %) clay-rich bedrock aquifers. This supports the assumption, used for subsequent modelling of residence times, that bedrock effective porosities may reasonably be assumed as equal to Waxman and Smits porosities.

Aquifer recharge

Application of the water table fluctuation using *Sy* values derived from MRS provided recharge values that vary along the hillslope (Table 4), from an average of 163 mm/y in the hillslope to an average of 287 mm/y in the valley bottom, which correspond to about 10% and 20% or the rainfall, respectively. These values are higher than previous values reported by Cai & Ofterdinger (2016) due to estimated *Sy* values higher than the literature values used by previous authors.

Data integration and numerical groundwater modelling

Methods

A 2D numerical groundwater model (equivalent porous medium EPM) was constructed in line with the ERT transect in order to assess the influence of the structural heterogeneity, i.e. the spatial variations in flow (permeability, anisotropy) and storage (porosity) properties on groundwater flow paths and residence time. EPM models are commonly used for studying groundwater dynamics in fractured bedrock aquifers at catchment and hillslope-scale (Ball *et al*. 2014; Welch & Allen 2014; Kolbe *et al*. 2016). EPM models use integrated hydraulic properties data (hydraulic conductivities, storativities) from hydraulic test solutions and anisotropy analysis (which are also EPM models). They are also a lot less computationally expensive than discrete fracture network (DFN) models for which the current hillslope-scale knowledge on the actual distribution and properties (length, aperture, roughness) of fracture networks is insufficient for DFN model application.

We used the finite element code FEFLOW v6.2. The model domain was 2D vertical (cross section; Fig. 8) with a length slightly shorter than the ERT transect (1200 m; the ERT region south of the river was not included). The ground surface was obtained from the DEM and therefore identical to the ERT profile. The maximum elevation (NW of transect) was 183 m and the minimum river elevation (SW of transect) was 31.5 m, i.e. the elevation of the river. The base of the model was fixed at -50 m relative to mean sea level. The mesh comprised 5366 triangular elements and 2974 nodes.

The model domain was structured in five layers: alluvium (only present in the floodplain), broken bedrock, fissured bedrock, massive bedrock, and a hypothetical very low conductivity/porosity bottom layer (Figure 8), within which homogeneous hydrogeological parameters were applied. Two alternative numerical models were applied using different levels of hydrogeological knowledge of the site (aquifer structure, hydraulic properties, and recharge). Model 1 used the information obtained from boreholes only. It considered a uniform layered structure defined from lateral interpolation of the hydrogeological units as identified in boreholes and initially interpreted by Moe *et al*. (2010) prior to extensive deployment of geophysical surveys. This model represents the common, most simple catchment/regional scale conceptualisation of basement aquifers (Fig. 8a). Model 2 incorporated the additional knowledge obtained from the interpretation of geophysical surveys (Fig. 8b). Comparing the two models aimed at illustrating the added value provided by the geophysical data. Details of the set up of both models were as follows.

Model 1 considered a tabular spatial distribution of the different aquifer units that mimics the topography (Figure 8a). Recharge values were based on borehole-based estimates by Cai & Ofterdinger (2016). Model hydraulic conductivities and porosities were assigned from layer-specific hydraulic test results from Moe et al. (2010) and Comte *et al*. (2012), respectively (Table 5). Effective porosities, used for residence time calculations, were assumed to be equal to the specific yield values (*Sy*) from borehole data. As Model 1 initially provided a poor fit to observed groundwater heads, a recalibration had to be performed through increasing recharge (x5) and decreasing hydraulic conductivities (/5).

Model 2 was based on the geometry of the different aquifer units from the interpretation of the geophysical data (ERT and MRS). Recharge values were the new values calculated with the water table fluctuation method using the specific yield data derived from the MRS surveys (see Section *Aquifer characterisation*). Hydraulic conductivities *K* (Table 5) were applied as anisotropic and assigned from joint interpretation of revised hydraulic test data Comte *et al*. (2012), geophysical data and fracture analyses (see Section *Aquifer characterisation*). Effective porosities (Table 5) were assigned using the porosity values obtained from joint application of ERT and MRS (Figure 7 and Table 5).

Both models were assigned values of longitudinal and transversal dispersivity of 30 and 3 m respectively, as typically reported for fractured aquifers for the scale of this study (hundreds of m to km-scale flow paths; Neuman 2005; Schulze-Makuch 2005; Zhou *et al*. 2007). With regard to the boundary conditions other than the recharge described above, both models also computed the top surface as a seepage face, with recharge (entering flux) switching automatically to discharge (exiting flux) during simulations when the water table was equal or higher than the top surface. Additionally, the river was applied as a constant head of 31.5 m, which is the average observed river level. In terms of groundwater ages, water entering from recharge was assigned a constant age of 0 years.

Models were run in transient flow and age conditions with initial heads equal to the topographic elevation and initial ages of 0 years, until reaching a dynamic steady state. Flow and groundwater age were solved simultaneously. Groundwater age simulations in FEFLOW are treated as dissolved transport and account for the applied values of effective porosities and dispersivities. This, contrary to isochrone calculations on flow paths (streamlines), allows for water dispersion and mixing of groundwater ages. Flow path simulations were run on simulated flow fields to highlight average flow paths from recharge (top surface) to discharge points (river and seepage areas).

Numerical modelling results

Models evaluation

The goodness-of-fit of the different models, i.e. the discrepancy between predicted and observed heads was assessed through root-mean-square error (RMSE) calculations. Model 1, which computed previously published values of hydraulic properties (Moe *et al*. 2010) and recharge (Cai & Ofterdinger 2016) initially failed to reproduce hydraulic heads that fit the observed head in the boreholes. Calculated head values were significantly lower than observed, of up to 125 m difference at GO1 (uphill), due to either underestimation of the recharge or overestimation of the aquifer hydraulic conductivities, but close to observations downhill due to the constraint by the river fixed head. Across the whole transect this model produced a high total RMSE of 71.6 m. The recalibration of Model 1, through increasing the recharge and decreasing *K* both by a factor five, produced a reasonable fit with a RMSE of 3.7 m. Models 2 directly reproduced reasonably well the hydraulic heads observed in the boreholes GO1, GO2 and GO3 with a RMSE of 4.0 m. For Model 2 however, the simulated heads in the deep GO1 and GO2 boreholes were somewhat higher than those

observed. Because these two boreholes are within or close to deep weathered/fractured zones (as identified by geophysics), a 3D model allowing deep and lateral drainage would be expected to correct for this mismatch by lowering heads in the deep units. The model comparison demonstrates that both Model 1 (final recalibrated version) and Model 2 equally honour the observed heads, however only Model 2 also honours the observed aquifer properties, structure and recharge values.

Simulation of groundwater fluxes, flow paths and residence time distributions

For both Model 1 and Model 2, Darcy's fluxes were highest in the broken bedrock and decreased with depth (Fig. 9a,d). The deep weathered/fractured zones identified by geophysics and computed in Model 2 allowed for thicker areas of high flux (Fig. 9d), especially in the vicinity of these zones (X 300-600 m; 750-850 m; 110-1300 m). In terms of budget (Fig. 10), in the case of Model 1 almost 80 % of the flow rate in the aquifer, originating from the recharge, transited through the broken bedrock layer (transition zone) and fissured layer (shallow zone), with over 60% in the broken bedrock only. The proportion was lower for Model 2, with about 70% flowing through broken and fissured bedrock and about 50% through the broken bedrock only. This suggests that overall hydrogeological heterogeneity favours deeper groundwater flow in the fissured and massive bedrock (< 20 % for Model 1 vs. about 25 % for Model 2).

This is further confirmed by the average flow path (streamlines) simulations (Fig. 9b,e). In the case of Model 1, most flow paths were sub-horizontal and restricted to the shallow broken layer (Fig. 9b). A limited number of flowlines travel through the fissured and massive layers. For Model 2, which incorporated lateral variations in the thickness of the aquifer layers, flow paths were more evenly distributed with depth, with higher contributions from the fissured and massive layers (Fig. 9e). They were also characterised by undulations as a result of lateral variations of weathering thicknesses and the anisotropy of conductivity with an increased vertical component to the groundwater flow. In detail, Model 2 simulations showed sub-vertical or oblique groundwater flow from recharge locations where weathering/fracturing is poorly developed. In locations with extensive weathering/fracturing, groundwater directions changed upwards suggesting that these locations may act as drainage structures at catchment and regional scale. These model regions were also associated with groundwater discharge through seepage, which agree with the spring lines locations observed in the field (Fig. 4). Seepage appeared to occur specifically in areas where the two following conditions are met: (1) upwelling groundwater flow associated to decrease in thickness of the broken bedrock on the downgradient side of deep weathered/fractured 'channels' and (2) presence of topographic low also associated to less competent bedrock in these zones. In contrast the absence of deep weathering zones in Model 1 resulted in higher and more evenly spread seepage along the hillslope.

Groundwater age simulations for the two models (Fig. 9c,f and Fig. 11) provided ages increasing both laterally from hill top to the valley and with depth. Youngest groundwater was obtained in GO1T and GO3SS and oldest in GO3S, GO3D and GO2D (Fig. 11). Model 1 and Model 2 both resulted in simulated ages less than about 10 years and 50 years, respectively, in boreholes and seepages areas. When compared to Model 1, which did not incorporate lateral heterogeneity, Models 2 showed greater age mixing with depth whereas the former produced steeper age gradient with depth in the upper aquifer. Model 2 ages are consistent with independent Tritium data (Pilatova 2013) that showed (1) Tritium concentrations in boreholes within the range 2.5-17.6 TU reflecting a mixture of sub-modern water (< 1TU; prior 1952) and modern water (5-15+ TU, i.e. < 5 to 10 years) (Figure 11), (2) decreasing Tritium values with depth reflecting larger component of older waters with depth, (3) highest Tritium values (>14 TU) in the upper bedrock at GO1T well (X=~100 m) and GO2S well (X=~600 m) reflecting high proportion of young water associated to recharge as well as descending to sub-horizontal groundwater flow and (4) lowest Tritium values (2.5 TU) encountered at the deep GO3D well (X=~1200 m) reflecting larger component of older upwelling groundwater.

The distribution of residence times obtained for Model 2, the best parameterised model accounting for the geophysical heterogeneity, is also broadly consistent with previous catchment- or

hillslope-scale studies in fractured hard rock aquifers. Robins & Smedley (1994) reported modern groundwater tritium ages in the fractured basement of Jersey. Jaunat *et al*. (2012) reported CFC-SF6 residence times lower than 50 years in weathered/fractured gneiss of the French Basque Country for similar flow path lengths. Banks *et al*. (2009) reported CFC ages of less than 40 years in a hillslope transect underlain by weathered/fractured metasediments. Lapworth *et al*. (2013) reported CFC-SF6-3H mean residence times of 32-65 years in deeply weathered catchments of the West African basement. Kolbe *et al*. (2016) modelled mean transit times of 40 years in a granite-gneiss catchment of ~10 km-long with similar mean flow path lengths of ~300 m. The modelling results also corroborate recent findings by Ameli *et al.* (2016) who showed the major impact of subsurface heterogeneity on groundwater residence time distribution in a well-studied hillslope transect in glacial till in Sweden.

General discussion

Study implications for groundwater resilience to climate change and contaminants, and catchment management approaches

The results indicate that overall low and depth-decreasing porosities, together with high hydraulic gradients, give relatively short residence times for groundwater from recharge to seepage or river discharge. In the upper bedrock (broken bedrock/transition zone; 1 to 30 m thick), where over 50% of groundwater flow occurs, models results suggest groundwater flow paths of between 10-100 m long and groundwater ages of < 1 year. This implies that groundwater in this aquifer unit is sensitive to both weather seasonality and extreme events (winter/summer recharge condition and drought/floods). This groundwater mostly contributes to diffuse seepage, which is then collected by agricultural drains. As such, point and diffuse contaminants in groundwater are expected to affect surface water quickly, on timescales of days to months. In the deeper bedrock (fissured/shallow and massive/deep bedrock; depths higher than 10-50 m), model results yield longer flow paths (100-1000 m) and older groundwater ages (from one year to several decades). This implies higher groundwater resilience to extreme weather conditions, seasonality and incidental contaminant exposures, but not to long-term (multi-decadal) climate change and persistent contamination, such as (i) changes in recharge due to long-term changes in rainfall and evapotranspiration and (ii) diffuse (e.g. agricultural nutrients) contamination. As these deeper bedrock units mostly contribute to river flow as well as the most significant seepages areas/drains, the surface water network at base flow (i.e. when mostly supported by groundwater) is also expected to be more vulnerable to long-term climate change and contamination.

Model comparison (Model 1 vs. Model 2) further highlights the importance of adequately accounting for aquifer heterogeneity when using models to predict the response of weathered/fractured rock catchments to climate and land use change as well as contaminations. Using information from borehole observations only, which does not allow for adequately capturing spatial variations in weathering/fracturing, leads to underestimation of the contribution of deep aquifer units to catchment water balance and discharge to river/surface water bodies. This also leads to underestimating groundwater residence times and exaggerating both ground and surface water sensitivity to climate variability and contaminations. In contrast, better accounting for aquifer heterogeneity as revealed here by geophysical surveys, results in higher resilience of groundwater resources to climate variability and surface contaminations. This is of importance when applying groundwater models with the aim of accurately informing short to long-term catchment management and policy.

Study limitations and implications for residence time distributions

The hydrogeophysical and numerical modelling works conducted in this study reveal the major role played by hydrogeological heterogeneities on groundwater flowpaths and transit time distributions at 2D hillslope scale providing important insights into catchment scale groundwater processes in weathered/fractured aquifers. The methodology however has some limitations with respect to accurately representing 3D heterogeneities and their influence on flow and transit times at smaller (i.e. borehole) or larger (i.e. catchment or region). Specifically, the hillslope characterisation and modelling work conducted do not represent; (1) three-dimensional groundwater flow such as lateral or deep drainage due to deep weathering structures possibly significant at the catchment/regional scale; (2) individual fracture networks and associated fracture flow processes; (3) accurate 2D/3D clay distribution and cementation factor; (4) uncertainty in estimates of hydrogeological porosity from geophysical (ERT and MRS) porosity; (5) temporal variability in recharge; (6) flow processes in the unsaturated zone above the water table.

With regards to the two-dimensionality of the models, it may be expected that some groundwater flow at the catchment scale may take place laterally to the 2D transects especially (i) in deep weathering furrows such as these detected by geophysics at about 300-600m, 750-850m and 110-1300m; (ii) in more local preferential flow paths along the NE-SW fractured systems. Not accounting for these 3D processes, the current modelling approach is likely to lead to underestimate deep groundwater flow as well as mixing and resulting groundwater ages, and overestimate seepage (along the hillslope). Full 3D geophysical (acquisition and inversion) and numerical modelling approaches are recommended in basement catchments where strong 3D heterogeneity is expected. The expected increased accuracy is however at the cost of much higher requirement in terms of acquisition and modelling time and resource, including computational.

Increased accuracy in modelling results may also be obtained by implementing discrete fractured network (DFN) modelling approaches. The structural and geophysical data may be used to support the computation of fracture orientation and density, which would allow direct computation of fracture permeability and aperture. A DFN approach requires implementation of computationally expensive 3D models.

Application of ERT to derive porosities requires information on spatial variations of bedrock clay content and clay mineralogy. Direct and high resolution 3D characterisation of clay properties through sampling/coring is challenging, but such resolution may be achieved indirectly through use of alternative geophysical methods such as the induced polarisation (IP).

In line with previous works in similar settings, we have assumed that aquifer effective porosity was half the MRS water content and equal to ERT porosity. Should this assumption be erroneous, effective porosity values higher than the ERT total porosity would result in higher groundwater residence times. More research is recommended to constrain the relationship between ERT/MRS porosity and hydrogeological porosities (storativity and effective porosity).

The temporal variability in recharge has not been accounted for and would be required to better understanding seasonality in groundwater contribution to seepage, drains and stream. It may, in addition, enhance groundwater mixing and, therefore groundwater residence times. Similarly, neglecting flow processes in the unsaturated zone primarily result in underestimating groundwater mixing and ages in areas where the unsaturated zone is thicker.

Conclusion

The study highlights the strong control of geological heterogeneities on groundwater flow and residence times in metamorphic rock catchments in temperate regions. It also demonstrates the high value of surface geophysical data and fracture and clay analysis for the parametrisation of numerical groundwater models in complex aquifers.

The investigations have revealed a high degree of heterogeneity in the distribution of hydrogeological properties at the hillslope scale. Through 2D equivalent porous media modelling using FEFLOW, it has been shown that the high spatial variation of hydraulic conductivity and porosity results in deeper groundwater flow paths (with an increased in the vertical flow component with depth) as compared to simple layered conceptual models based on borehole data only. They also result in older groundwater ages through enhanced mixing and dispersion caused by heterogeneities and anisotropies of hydraulic conductivity. Groundwater ages along the hillslope were simulated to be of modern ages, i.e. less than 50 years, consistent with available Tritium data.

The integrated approach presented, using both borehole and surface geophysical surveys, is shown to help parametrise numerical groundwater models that honour the observed data without requiring significant parameter recalibration. Such robustly parameterised models offer straightforward application in catchment water management, to investigate in detail the contribution of groundwater to the catchment hydrological function, as well as the impact of climate change and contaminants on groundwater.

The results presented here suggest that the uppermost weathered/broken part of the aquifer, which is a major contributor to hillslope discharge, is sensitive to extreme hydrological events and seasonal climate fluctuations as well as point and diffuse contamination. The deeper, less weathered part of the aquifer is a significant contributor to river flow and major hillslope seepage areas and would be more sensitive to long-term (decadal) climate fluctuations and persistent, diffuse contaminants.

It is suggested that the 2D steady-state hillslope approach conducted provides only a minimum estimate of groundwater ages at the catchment scale. This is due to underestimation of groundwater mixing favoured by possible 3D structures and seasonal recharge. Full 3D characterisation and modelling approaches, although more expensive in terms of data and computational resources, are required to further improve our understanding of groundwater flow and residence times. Recommendations include: (1) implementation of 3D MRS and ERT surveys and inversion, including 3D characterisation of clay mineralogy through alternative geophysical methods such as IP; (2) resolution and computation of fracture networks and fracture flow; (3) application of transient, variably saturated model for better accounting of mixing and processes in the unsaturated zone; (4) more research on the relationship between geophysical (ERT and MRS) porosity and hydrogeological porosity.

Acknowledgements

We acknowledge the valuable assistance provided by Harold Cole in Gortinlieve for access to his properties, practical and technical help as well as the MSc students at QUB for data collection and processing. This work is based on a research grant aided by the Irish Department of Communications, Energy and Natural Resources under the National Geoscience Programme 2007–2013 and the Geological Survey of Ireland Geoscience Research Programme 2015-2016. MRS works benefited from complementary support by the French Research Council (ANR): project Labex OSUG@2020 (ANR-10-LABX-56) and project EQUIPEX CRITEX (ANR-11-EQPX-0011) for providing the MRS equipment. The views expressed are the authors' own and do not necessarily reflect the views and opinions of the Minister for Communications, Energy and Natural Resources. Comments by two anonymous reviewers and corresponding editor Alan MacDonald are greatly appreciated and helped improving the final manuscript.

References

Ameli, A.A., Amvrosiadi, N., Grabs, T., Laudon, H., Creed, I.F., McDonnell, J.J. & Bishop, K. 2016. Hillslope permeability architecture controls on subsurface transit time distribution and flow paths, *Journal of Hydrology*, **543**, 17–30, https://doi.org/10.1016/j.jhydrol.2016.04.071

Archie, G.E. 1942. The electrical resistivity log as an aid in determining some reservoir characteristics, *Transactions of the AIME*, **146**(01), 54–62, https://doi.org/10.2118/942054-G

Ball, L.B., Caine, J.S. & Ge, S. 2014. Controls on groundwater flow in a semiarid folded and faulted intermountain basin, *Water Resources Research*, **50**(8), 6788–6809, http://dx.doi.org/10.1002/2013WR014451

Baltassat, J.M., Legchenko, A., Ambroise, B., Mathieu, F., Lachassagne, P., Wyns, R., Mercier, J.L. & Schott, J.J. 2005. Magnetic resonance sounding (MRS) and resistivity characterisation of a mountain hard rock aquifer: the Ringelbach Catchment, Vosges Massif, France, *Near Surface Geophysics*, **3**(4), 267–274

Banks, E.W., Simmons, C.T., Love, A.J., Cranswick, R., Werner, A.D., Bestland, E.A., Wood, M. & Wilson, T. 2009. Fractured bedrock and saprolite hydrogeologic controls on groundwater/surface-water interaction: a conceptual model (Australia), *Hydrogeology Journal*, **17**(8), 1969–1989, https://doi.org/10.1007/s10040-009-0490-7

Boucher, M., Favreau, G., Vouillamoz, J.M., Nazoumou, Y. & Legchenko, A. 2009. Estimating specific yield and transmissivity with magnetic resonance sounding in an unconfined sandstone aquifer (Niger), *Hydrogeology Journal*, **17**(7), 1805–1815, https://doi.org/10.1007/s10040-009-0447-x

Cai, Z. & Ofterdinger, U. 2016. Analysis of groundwater-level response to rainfall and estimation of annual recharge in fractured hard rock aquifers, NW Ireland, *Journal of Hydrology*, **535**, 71–84, https://doi.org/10.1016/j.jhydrol.2016.01.066

Carroll, D. 1959. Ion exchange in clays and other minerals, *Geological Society of America Bulletin*, **70**(6), 749–779, https://doi.org/10.1130/0016-7606(1959)70[749:IEICAO]2.0.CO;2

Cassidy, R., Comte, J.C., Nitsche, J., Wilson, C., Flynn, R. & Ofterdinger, U. 2014. Combining multi-scale geophysical techniques for robust hydro-structural characterisation in catchments underlain by hard rock in post-glacial regions, *Journal of hydrology*, **517**, 715–731, https://doi.org/10.1016/j.jhydrol.2014.06.004

Caulfield, J., Chelliah, M., Comte, J.C., Cassidy, R. & Flynn, R. 2014. Integrating petrography, mineralogy and hydrochemistry to constrain the influence and distribution of groundwater contributions to baseflow in poorly productive aquifers: Insights from Gortinlieve catchment, Co. Donegal, NW Ireland, *Science of the Total Environment*, **500**, 224–234, https://doi.org/10.1016/j.scitotenv.2014.08.105

Chandra, S., Dewandel, B., Dutta, S. & Ahmed, S. 2010. Geophysical model of geological discontinuities in a granitic aquifer: Analyzing small scale variability of electrical resistivity for groundwater occurrences, *Journal of Applied Geophysics*, **71**(4), 137–148, https://doi.org/10.1016/j.jappgeo.2010.06.003

Chew, D.M. 2009. Grampian orogeny. *In*: Holland, C.H. & Sanders, I.S. (eds) *The geology of Ireland*. Dunedin, Edinburgh, 69–93.

Comte, J.C., Cassidy, R., Nitsche, J., Ofterdinger, U., Pilatova, K. & Flynn, R. 2012. The typology of Irish hard-rock aquifers based on an integrated hydrogeological and geophysical approach, *Hydrogeology Journal*, **20**(8), 1569–1588, https://doi.org/10.1007/s10040-012-0884-9

Cooper, M.R., Anderson, H., Walsh, J.J., Van Dam, C.L., Young, M.E., Earls, G. & Walker, A. 2012. Palaeogene Alpine tectonics and Icelandic plume-related magmatism and deformation in Northern Ireland, *Journal of the Geological Society*, **169**(1), 29–36, https://doi.org/10.1144/0016-76492010-182

Crain, E.R. (eds) 2000. *Crain's petrophysical handbook*. Spectrum.

Daly, D., Deakin, J., Craig, M., Mockler, E.M., et al. 2016. Progress in Implementation of the Water Framework Directive in Ireland. International Association of Hydrogeologists (IAH) (Irish Group) Sustaining Ireland's Water Future: The Role of Groundwater, Tullamore, Co. Offaly, Ireland, 12-13 April 2016.

DCCAE 2017. Groundwater, Department of Communications, Climate Action and Environment, Government of Ireland. http://www.dccae.gov.ie/en-ie/natural-resources/topics/Geological-Survey-of-Ireland/groundwater/Pages/Groundwater.aspx

Day-Lewis, F.D., Slater, L.D., Robinson, J., Johnson, C.D., Terry, N. & Werkema, D. 2017. An overview of geophysical technologies appropriate for characterization and monitoring at fractured-rock sites, *Journal of Environmental Management*, **204**, 709–720, https://doi.org/10.1016/j.jenvman.2017.04.033

De Marsily, G., Delay, F., Goncalves, J., Renard, P., Teles, V. & Violette, S. 2005. Dealing with spatial heterogeneity, *Hydrogeology Journal*, **13**(1), 161–183, https://doi.org/10.1007/s10040-004-0432-3

Descloitres, M., Ruiz, L., Sekhar, M., Legchenko, A., Braun, J.J., Kumar, M. & Subramanian, S. 2008. Characterization of seasonal local recharge using electrical resistivity tomography and magnetic resonance sounding, *Hydrological Processes*, **22**(3), 384–394, http://dx.doi.org/10.1002/hyp.6608

Ellis, D.V. & Singer, J.M. 2007. *Well logging for earth scientists*. Dordrecht, Springer.

EPA 2006. Ireland; Water Framework Directive, Monitoring Programme prepared to meet the requirements of the EU Water Framework Directive (2000/60/EC) and National Regulations implementing the Water Framework Directive (S.I. No. 722 of 2003) and National Regulations implementing the Nitrates Directive (S.I. No. 788 of 2005), Environmental Protection Agency, Co. Wexford, Wexford, Ireland

Francés, A.P., Lubczynski, M.W., Roy, J., Santos, F.A. & Ardekani, M.R.M. 2014. Hydrogeophysics and remote sensing for the design of hydrogeological conceptual models in hard rocks–Sardón catchment (Spain), *Journal of Applied Geophysics*, **110**, 63–81, https://doi.org/10.1016/j.jappgeo.2014.08.015

Gillespie, M.R., Kemp, S.J., Vickers, B.P., Waters, C. & Gowing, C.J. 2001. *Cation-exchange capacity (CEC) of selected lithologies from England, Wales and Scotland*, SEPA R&D Technical Report, **P2-222/TR**.

Hartmann, D.J. & Beaumont, E.A. 1999. *Predicting reservoir system quality and performance. Exploring for oil and gas traps*. AAPG Treatise of Petroleum Geology, Handbook of Petroleum Geology.

Healy, R.W. & Cook, P.G. 2002. Using groundwater levels to estimate recharge, *Hydrogeology journal*, **10**(1), 91–109, https://doi.org/10.1007/s10040-001-0178-0

Henn, F., Durand, C., Cerepi, A., Brosse, E. & Giuntini, J.C. 2007. DC conductivity, cationic exchange capacity, and specific surface area related to chemical composition of pore lining chlorites, *Journal of colloid and interface science*, **311**(2), 571–578, https://doi.org/10.1016/j.jcis.2007.02.062

Hertrich, M., Green, A.G., Braun, M. & Yaramanci, U. 2009. High-resolution surface NMR tomography of shallow aquifers based on multioffset measurements, *Geophysics*, **74**(6), G47–G59, https://doi.org/10.1190/1.3258342

Holbrook, W.S., Riebe, C.S., Elwaseif, M., Hayes, J.L., Basler-Reeder, K., Harry, D.L., Malazian, A., Dosseto, A., Hartsough, P.C. & Hopmans, J.W. 2014. Geophysical constraints on deep weathering and water storage potential in the Southern Sierra Critical Zone Observatory, *Earth Surface Processes and Landforms*, **39**(3), 366–380, http://dx.doi.org/10.1002/esp.3502

Jaunat, J., Huneau, F., Dupuy, A., Celle-Jeanton, H., Vergnaud-Ayraud, V., Aquilina, L., Labasque, T. & Le Coustumer, P. 2012. Hydrochemical data and groundwater dating to infer differential flowpaths through weathered profiles of a fractured aquifer, *Applied geochemistry*, **27**(10), 2053–2067, https://doi.org/10.1016/j.apgeochem.2012.06.009

Kolbe, T., Marçais, J., Thomas, Z., Abbott, B.W., de Dreuzy, J.R., Rousseau-Gueutin, P., Aquilina, L., Labasque, T. & Pinay, G. 2016. Coupling 3D groundwater modeling with CFC-based age dating to classify local groundwater circulation in an unconfined crystalline aquifer, *Journal of Hydrology*, **543**, 31–46, https://doi.org/10.1016/j.jhydrol.2016.05.020

Lapworth, D.J., MacDonald, A.M., Tijani, M.N., Darling, W.G., Gooddy, D.C., Bonsor, H.C. & Araguás-Araguás, L.J. 2013. Residence times of shallow groundwater in West Africa: implications for hydrogeology and resilience to future changes in climate, *Hydrogeology Journal*, **21**(3), 673–686, https://doi.org/10.1007/s10040-012-0925-4

Legchenko, A. (eds.) 2013. *Magnetic resonance imaging for groundwater*. John Wiley & Sons.

Legchenko, A.V. & Shushakov, O.A. 1998. Inversion of surface NMR data, *Geophysics*, **63**(1), 75–84, https://doi.org/10.1190/1.1444329

Legchenko, A., Comte, J.C., Ofterdinger, U., Vouillamoz, J.M., Lawson, F.M.A. & Walsh, J. 2017. Joint use of singular value decomposition and Monte-Carlo simulation for estimating uncertainty in surface NMR inversion, *Journal of Applied Geophysics*, **144**, 28–36, https://doi.org/10.1016/j.jappgeo.2017.06.010

Legchenko, A., Descloitres, M., Vincent, C., Guyard, H., Garambois, S., Chalikakis, K. & Ezersky, M. 2011. Three-dimensional magnetic resonance imaging for groundwater, *New Journal of Physics*, **13**(2), 025022, https://doi.org/10.1088/1367-2630/13/2/025022

Legg, I.C., Pyne, J.F., Nolan, C., McCardle, P., Flegg, A.M & O'Connor, P.J. 1985. *Mineral localities in the Dalradian and associated igneous rocks of county Donegal, Republic of Ireland, and of Northern Ireland*. Geological Survey of Ireland report series **RS 85/3**.

Long C.B., MacDermot C.V., Morris J.H. *et al*. 1992. *Geology of North Mayo*. GSI 1:100,000 bedrock Series, Sheet 6 map and report, GSI, Dublin

Lubczynski, M. & Roy, J. 2004. Magnetic resonance sounding: New method for ground water assessment, *Groundwater*, **42**(2), 291–309, http://dx.doi.org/10.1111/j.1745-6584.2004.tb02675.x

McConnell B.J. & Long C.B. 1997. *Geology of North Donegal: a geological description to accompany the Bedrock Geology 1:100,000 Scale Map Series*. Sheet 1 and part of Sheet 2, North Donegal, GSI, Dublin

Moe H., Craig M. & Daly D. 2010. *Poorly productive aquifers: monitoring installations and conceptual understanding*. CDM and the Environmental Protection Agency, Dublin.

Nitsche, J. 2014. *Physical characterisation of groundwater flow systems of selected poorly productive bedrock aquifers in Ireland*. PhD thesis, Queen's University Belfast, 248 p. + appendixes.

Neuman, S.P. 2005. Trends, prospects and challenges in quantifying flow and transport through fractured rocks, *Hydrogeology Journal*, **13**(1), 124–147, https://doi.org/10.1007/s10040-004-0397-2

Pilatova, K. 2013. *Characterisation of Irish poorly productive aquifers using chemical and isotopic tools*. PhD thesis, Queen's University Belfast, 332 p.

Rayner, S.F., Bentley, L.R. & Allen, D.M., 2007. Constraining aquifer architecture with electrical resistivity imaging in a fractured hydrogeological setting, *Journal of Environmental & Engineering Geophysics*, **12**(4), 323–335, https://doi.org/10.2113/JEEG12.4.323

Revil, A., Cathles, L.M., Losh, S. & Nunn, J.A. 1998. Electrical conductivity in shaly sands with geophysical applications, *Journal of Geophysical Research: Solid Earth*, **103**(B10), 23925–23936, http://dx.doi.org/10.1029/98JB02125

Ridge, M.J. 1983. A Combustion Method For Measuring The Cation Exchange Capacity Of Clay Materials, *The Log Analyst*, **24**(03).

Robins, N.S. & Smedley, P.L. 1994. Hydrogeology and hydrogeochemistry of a small, hard-rock island—the heavily stressed aquifer of Jersey, *Journal of Hydrology*, **163**(3-4), 249–269, https://doi.org/10.1016/0022-1694(94)90143-0

Schulze-Makuch, D. 2005. Longitudinal dispersivity data and implications for scaling behaviour, *Groundwater*, **43**(3), 443–456, http://dx.doi.org/10.1111/j.1745-6584.2005.0051.x

Sharp, J.M. (eds.) 2014. *Fractured Rock Hydrogeology*. CRC Press.

Singh, A. 2014. Groundwater resources management through the applications of simulation modeling: a review, *Science of the Total Environment*, **499**, 414–423, https://doi.org/10.1016/j.scitotenv.2014.05.048

946 Singhal, B.B.S. & Gupta, R.P. (eds) 2010. *Applied hydrogeology of fractured rocks*. Springer Science &
947 Business Media.
948
949 Skinner, D. & Heinson, G. 2004. A comparison of electrical and electromagnetic methods for the
950 detection of hydraulic pathways in a fractured rock aquifer, Clare Valley, South Australia,
951 *Hydrogeology Journal*, **12**(5), 576–590, https://doi.org/10.1007/s10040-004-0356-y
952
953 Smith R.A. 1991. *Newtownards: memoir for sheet N37 and part of N38*. Geological map 1:50000
954 scale, British Geological Survey, Keyworth, UK
955
956 Swineford, A. 1955. *Petrography of Upper Permian Rock in South-central Kansas*. University of
957 Kansas.
958
959 Thomas, E.C. 1976. The determination of Qv from membrane potential measurements on shaly
960 sands, *Journal of Petroleum Technology*, **28**(09), 1087–1096, https://doi.org/10.2118/5505-PA
961
962 UKTAG 2011. UK Technical Advisory Group on the Water Framework Directive, Defining & Reporting
963 on Groundwater Bodies, Working Paper Version V6.21/Mar/2011
964
965 Vouillamoz, J.M., Sokheng, S., Bruyere, O., Caron, D. & Arnout, L. 2012. Towards a better estimate of
966 storage properties of aquifer with magnetic resonance sounding, *Journal of hydrology*, **458**, 51–58,
967 https://doi.org/10.1016/j.jhydrol.2012.06.044
968
969 Vouillamoz, J.M., Lawson, F.M.A., Yalo, N. & Descloitres, M. 2014. The use of magnetic resonance
970 sounding for quantifying specific yield and transmissivity in hard rock aquifers: The example of
971 Benin, *Journal of Applied Geophysics*, **107**, 16–24, https://doi.org/10.1016/j.jappgeo.2014.05.012
972
973 Waxman, M.H. & Smits, L.J.M. 1968. Electrical conductivities in oil-bearing shaly sands, *Society of*
974 *Petroleum Engineers Journal*, **8**(02), 107–122, https://doi.org/10.2118/1863-A
975
976 Welch, L.A. & Allen, D.M. 2014. Hydraulic conductivity characteristics in mountains and implications
977 for conceptualizing bedrock groundwater flow, *Hydrogeology Journal*, **22**(5), 1003–1026,
978 https://doi.org/10.1007/s10040-014-1121-5
979
980 Wiklander, L. 1964. Cation and anion exchange phenomena, *Chemistry of the Soil*, **126**, 107–148
981
982 Worthington R. & Walsh J.J. 2011. Structure of Lower Carboniferous basins of NW Ireland, and its
983 implications for structural inheritance and Cenozoic faulting, *Journal of Structural Geology*, **33**,
984 1285–1299, https://doi.org/10.1016/j.jsg.2011.05.001
985
986 Zhou, Q., Liu, H.H., Molz, F.J., Zhang, Y. & Bodvarsson, G.S. 2007. Field-scale effective matrix
987 diffusion coefficient for fractured rock: Results from literature survey, *Journal of contaminant*
988 *hydrology*, **93**(1), 161–187, https://doi.org/10.1016/j.jconhyd.2007.02.002

Tables and captions

Table 1. *Summary and source of Waxman and Smits model parameters used to derive porosity values for the different aquifer units*

	Bulk resistivity* [ohm.m]	Water temperature† [°C]	Water electrical conductivity† [S/m]	Cementation factor‡ [unitless]	Cation exchange capacity§ [meq/100g]
Overburden	< 500	12.1 – 16.0	0.027 – 0.045	2.5	2.0 – 6.0¶
Broken zone	500 – 2500	12.1 – 16.0	0.027 – 0.045	2.5	2.0 – 6.0
Fissured zone	300 – 1000	12.8 – 14.2	0.029 – 0.050	2	5.2 – 18.7
Massive zone	1000 – 10 000	12.7 – 13.1	0.033 – 0.057	1.5	1.2 – 1.7

* 2D distribution obtained from ERT (see Results section).
† average values (summer 2009) recorded in boreholes (low temporal variability).
‡ from Hartmann and Beaumont (1999).
§ values calculated from mineralogical analysis and natural gamma log (see Results section).
¶ same values as for the broken zone due to lack of in situ data.

Table 2. *Clay compositions in the different boreholes and resulting bedrock clay weight fraction and cation exchange capacity (CEC)*

	Muscovite* % vs tot. clay	Chlorite* % vs tot. clay	Illite* % vs tot. clay	Montm.* % vs tot. clay	Nat. γ† cps	Clay weight fraction‡ %	Total CEC‡ meq/100g
GO1							
Broken zone (transition)	58	27	7	8	116	51	6.0
Fissured zone (shallow)	40	20	22	18	111	51	**11.7**
Massive zone (deep)	66	34	0	0	102	43	1.7
GO2							
Broken zone (transition)	75	11	8	5	101	40	3.2
Fissured zone (shallow)	18	3	47	32	102	48	**18.7**
Massive zone (deep)	82	18	0	0	116	47	1.2
GO3							
Broken zone (transition)	77	14	5	4	78	30	2.0
Fissured zone (shallow)	28	5	40	27	41	16	**5.2**
Massive zone (deep)	82	18	0	0	116	47	1.2

* dominant clay minerals that affects natural gamma logging and rock bulk CEC. CEC (muscovite)~1 meq/g; CEC (illite)~10 meq/g; CEC (illite)~20 meq/g; CEC (montmorillonite)~90 meq/g (multiple sources, see Methods section).
†average natural gamma count per seconds from borehole logging.
‡ Clay weight fraction and CEC calculated from individual clay CEC and natural gamma according to Revil *et al*. (1998).

Table 3. *Summary of isotropic hydraulic conductivities obtained from pumping and recovery test interpretation and comparison with previous results*

Hydrogeological unit	Thickness from ERT [m]	Mean *K* [m/d]	*K* range [m/d]	Mean *K* from previous works* [m/d]	*K* range from previous works* [m/d]
Overburden	10 (in valley floor)	8.7	-	9	-
Broken bedrock (transition z.)	15-60	1.3×10^{-1}	$1\times10^{-1} – 2\times10^{-1}$	1	$7\times10^{-2} – 7$
Fissured bedrock (shallow z.)	5-40	1.0×10^{-2}	$3\times10^{-3} – 4\times10^{-2}$	$1\ 10^{-2}$	$1\times10^{-3} – 4\times10^{-2}$
Massive bedrock (deep z.)	>40	6.0×10^{-3}	$4\times10^{-3} – 8\times10^{-3}$	$1\ 10^{-2}$	$7\times10^{-3} – 6\times10^{-2}$

* initial hydraulic testing after drilling (Moe et al. 2010) using Horslev (infiltration tests) and Theis-Jacob (pumping tests)

Table 4. *Recharge values recalculated using the water table fluctuation methods and the specific yield values derived from MRS. Borehole name suffixes SS (subsoil), T (transition) are derived from the codes listed in section Hydrogeological setting*

	Rainfall* [mm/y]	Water table cumulated rise* [m]	Specific yield† [%]	Calculated recharge [mm/y]	Calculated recharge [% of rainfall]
Hillslope					
GO1T 2010-2011	1134	13.6	0.75	102	9
GO1T 2011-2012	1433	19.7	0.75	147	11
GO2T 2010-2011	1134	8.8	1.57	138	13
GO2T 2011-2012	1433	16.8	1.57	264	19
Average				163	13
Valley floor					
GO3SS 2010-2011	1134	7.4	3	222	21
GO3SS 2011-2012	1433	11.7	3	351	24
Average				287	23

* from Cai & Ofterdinger (2016)
† from MRS, assuming specific yield = 0.5*MRS water content

Table 5. *Details of key hydrogeological parameters and recharge values applied to Model 1 and 2*

	*Kmax** [m/d]	*Kmin*/*Kmax* [unitless]	Anisotropy angle [°]	Porosity† [%]	Recharge‡ [mm/y]
Model 1					
Overburden	9	1	Isotropic	20	Valley floor: 95 (480)§
Broken zone	1 (0.2)§	1	Isotropic	4	Hillslope: 75 (370)§
Fissured zone	0.01 (0.002)§	1	Isotropic	0.2	NA
Massive zone	0.01 (0.002)§	1	Isotropic	0.01	NA
Model 2					
Overburden	8.6	1	Isotropic	7	Valley floor: 285
Broken zone	0.14	0.5	75 ° dip NW	3	Hillslope: 165
Fissured zone	0.014	0.3	85 ° dip SE	0.1-0.5	NA
Massive zone	0.008	0.1	65 ° dip SE	0.01	NA

* from Moe *et al*. (2010) for Model 1; from Comte *et al*. (2012) for Model 2
† from Comte *et al*. (2012) for Model 1; from Waxman and Smits' model and MRS results for Model 2 (Figure 7)
‡ from Cai & Ofterdinger (2016) for Models 1; recalculated values for Model 2 (Table 4)
§ values in brackets are final values after model calibration to observed heads in boreholes (*K*/5 and Recharge*5)

Figure captions

Fig. 1. *Study site physical setting maps; (**a**) site location within the Irish basement geological framework (modified from Geological Survey of Ireland 2006); (**b**) catchment boundary with location of hydrological monitoring infrastructures; (**c**) local interpretative geological map with location of the borehole clusters, the ERT profile and the MRS soundings.(**a**) and (**b**) modified from Comte* et al*. (2012).*

Fig. 2. *Generic hydrogeological conceptual model of weathered/fractured rocks aquifers in the context of the Irish terminology (modified from Comte* et al*. 2012).*

Fig. 3. *Fracture pole density distributions (Schmidt net lower hemisphere projection) and orientations (fracture azimuth rose diagrams) from outcrops and boreholes (acoustic televiewer probe); blue points and arrows show the hydraulically active fractures unambiguously identified in boreholes (Nitsche 2014; modified from Comte* et al*. 2012)*.

Fig. 4. ERT results (**a**) and interpreted conceptual model of the weathered/fractured aquifer (**b**).

Fig. 5. *Comparison of hydraulic conductivities obtained from; (**a**) initial isotropic hydraulic test interpretations from Moe* et al*. (2010) used in Model 1; (**b**) refined isotropic interpretation from Comte* et al*. (2012); and (**c-e**) anisotropic* K *values used in Model 2, (**c**)* K_{max}*, (**d**)* $K_{equivalent}$*, and (**e**)* K_{min}*.*

Fig. 6. *Vertical distribution of MRS water content for the 8 MRS sounding (see locations on Figure 1) and comparison with the aquifer conceptual model units delineated from ERT (Figure 4)*.

Fig. 7. *Spatial variations of storage properties derived from ERT and MRS geophysical data; (**a**) ERT resistivity model with location of approximate volume of investigation of the MRS soundings; (**b**) MRS water content logs; (**c**) ERT porosity calculated from Waxman & Smits' model. Hatched areas indicate the unsaturated zone for which saturated Archie and Waxman & Smits models used are not applicable.*

Fig. 8. *Conceptual aquifer geometries implemented in the numerical models: (**a**) generic tabular structure of weathered/fractured layers from borehole interpretation (Model 1); (**b**) complex layered structure derived from geophysical data reconciled with borehole logs (Model 2). 1: Overburden (alluvial and glacial sediments); 2: Broken bedrock (transition zone); 3: Fissured (shallow) bedrock; 4: Massive (deep) bedrock; 5: Substratum (very low productivity).*

Fig. 9. *Simulation results for Model 1 (**a,b,c**) and Model 2 (**d,e,f**) showing groundwater seepage rates at the model surface, Darcy's fluxes variations across the transect (**a,d**), groundwater mean flowpaths (**b,e**), and groundwater ages (**c,f**).*

Fig. 10. *Relative distributions of groundwater flow rate (as % of total flow) in the four conceptual aquifer units (overburden, broken, fissured and massive bedrock) for the two models considered. The massive bedrock here also includes the deeper levels shown in Figure 8.*

Fig. 11. *Modelled groundwater ages in the different boreholes for the two model cases. The hatched area indicates groundwater ages that are older than the modern period of high atmospheric Tritium levels, and inconsistent with measured Tritium concentrations in boreholes samples.*

Figure 1

Click here to download Figure Figure1.tif

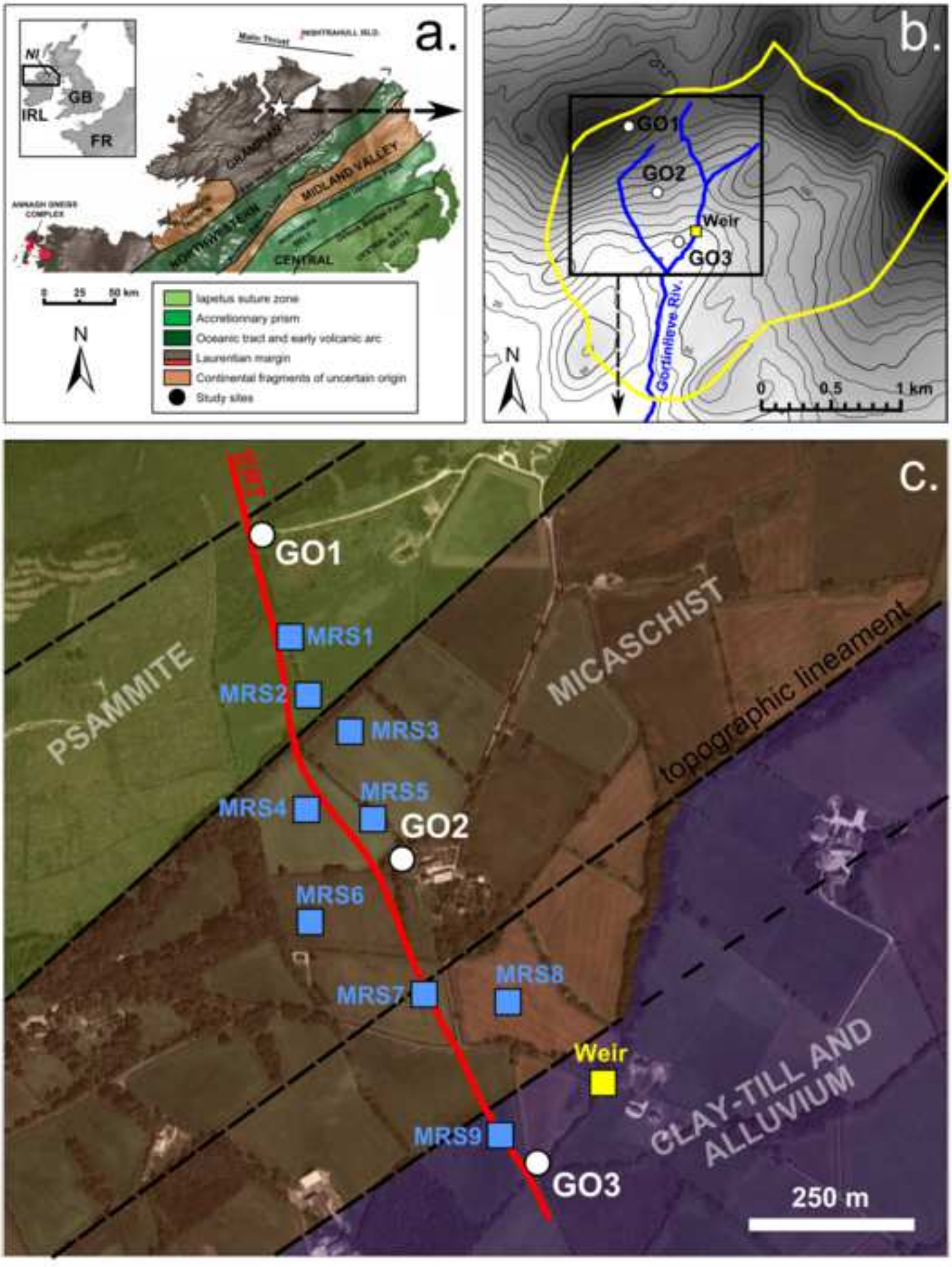

Figure 2

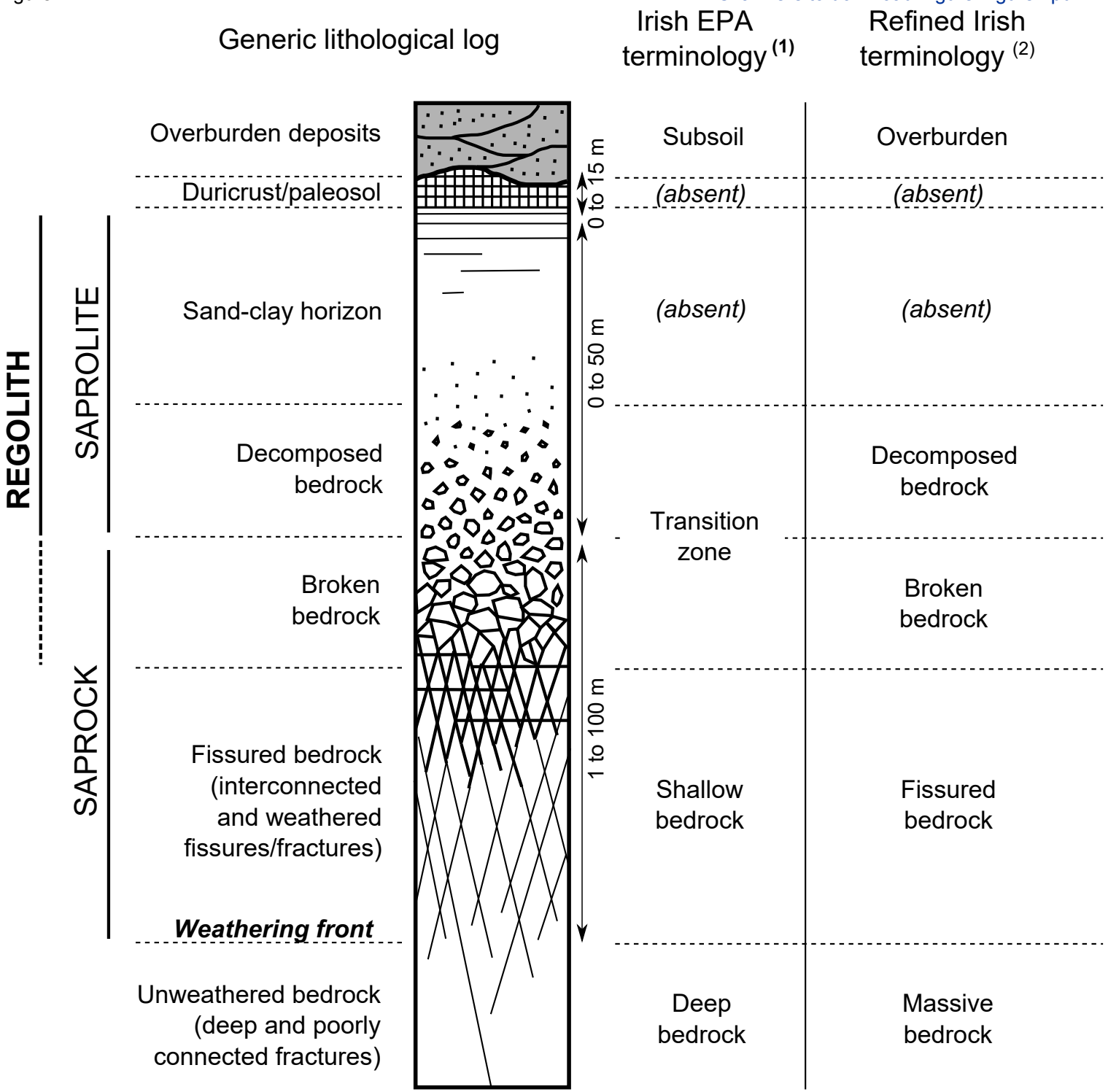

(1) After Moe *et al.* (2010)
(2) After Comte *et al*. (2012)

Figure 3

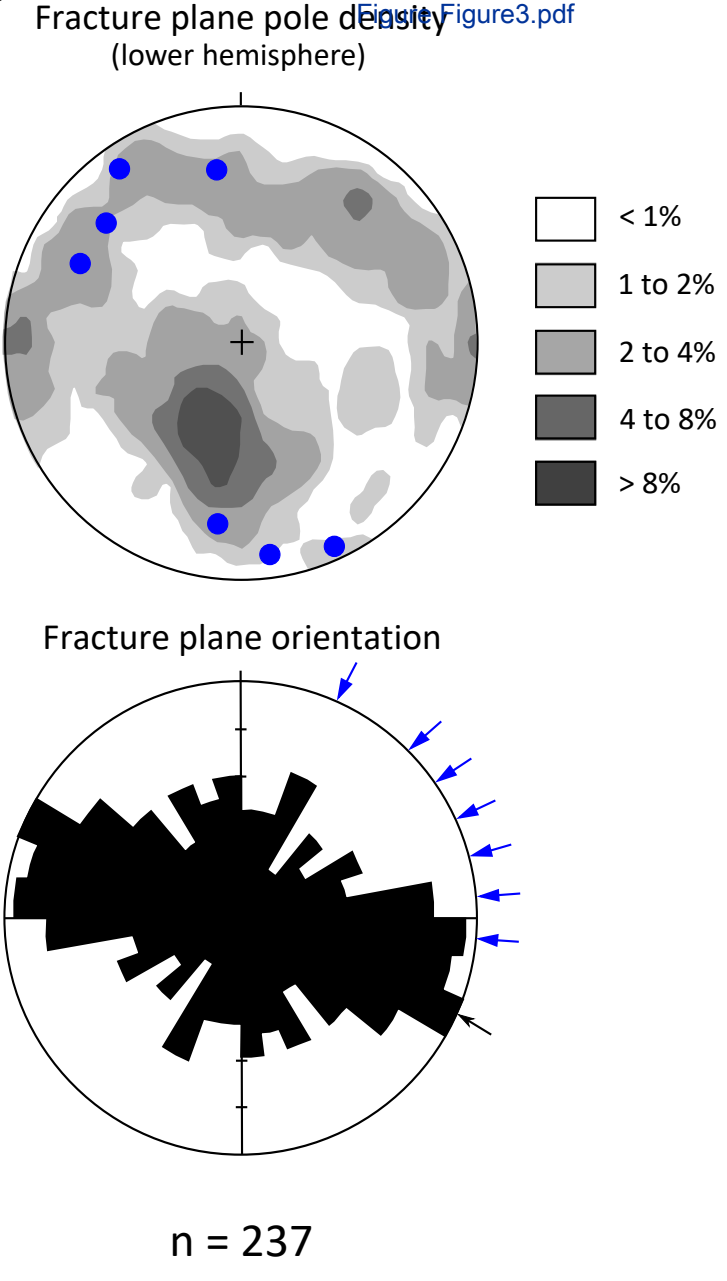

Figure 4

Click here to download Figure Figure4.pdf

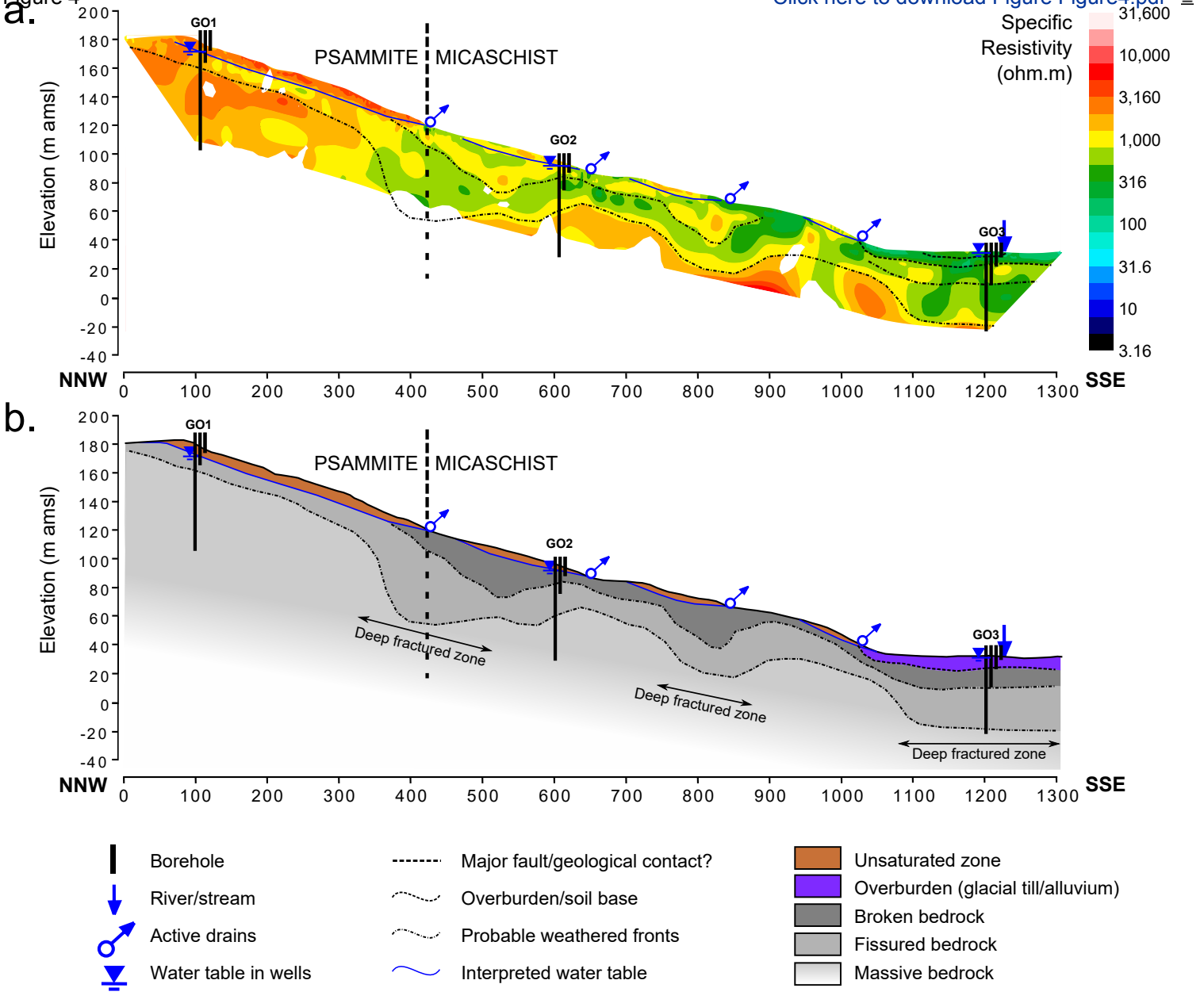

Figure 5

Click here to download Figure Figure5.tiff

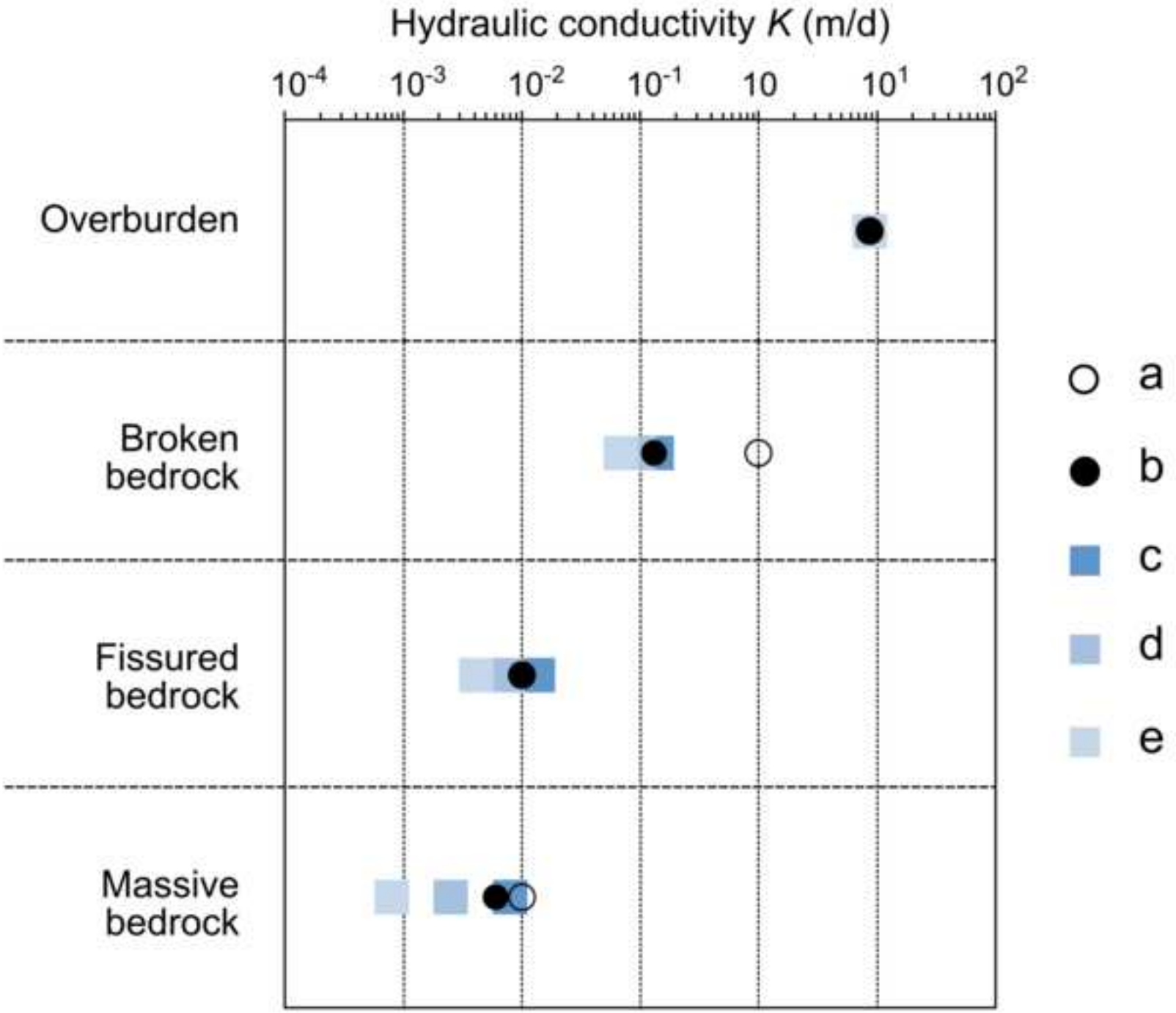

Figure 6

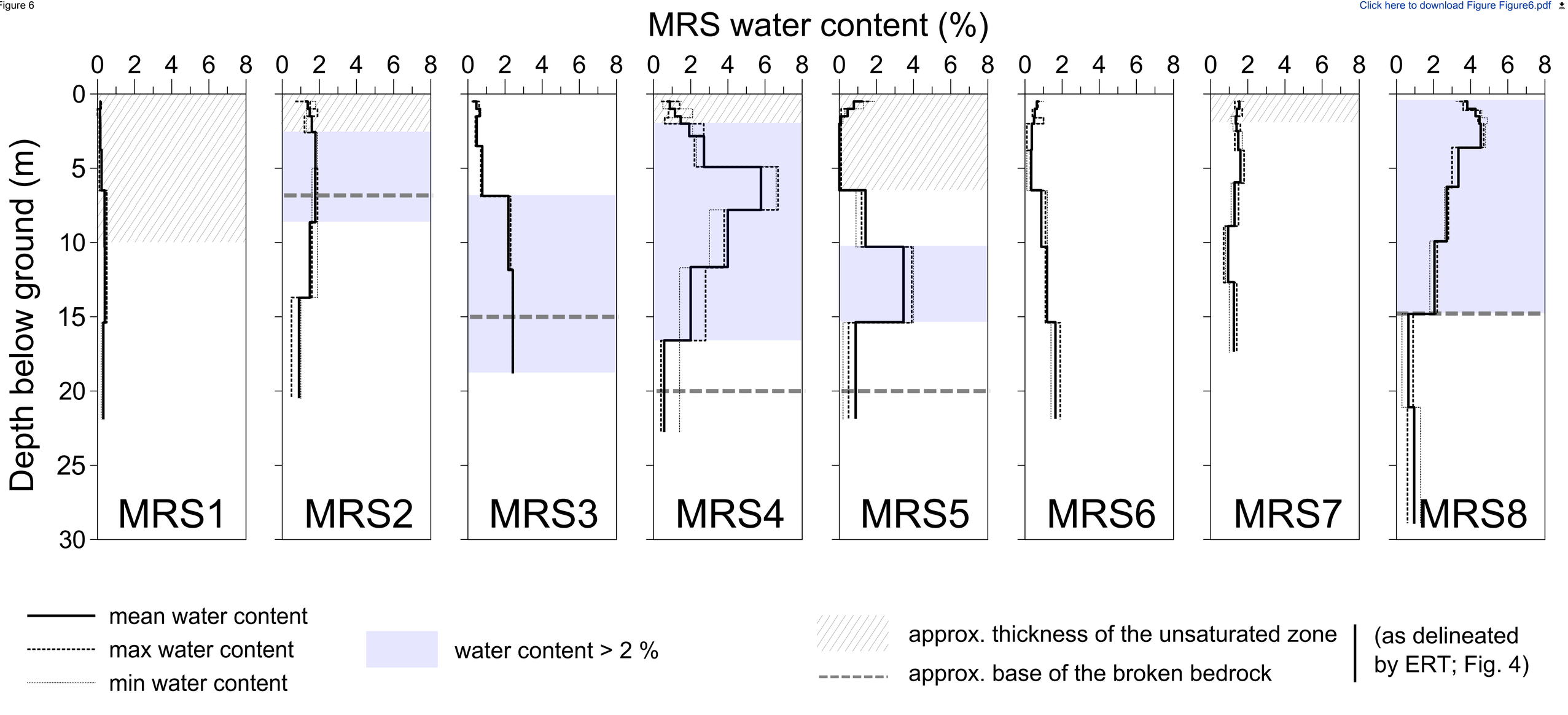

Figure 7

Click here to download Figure Figure7.pdf

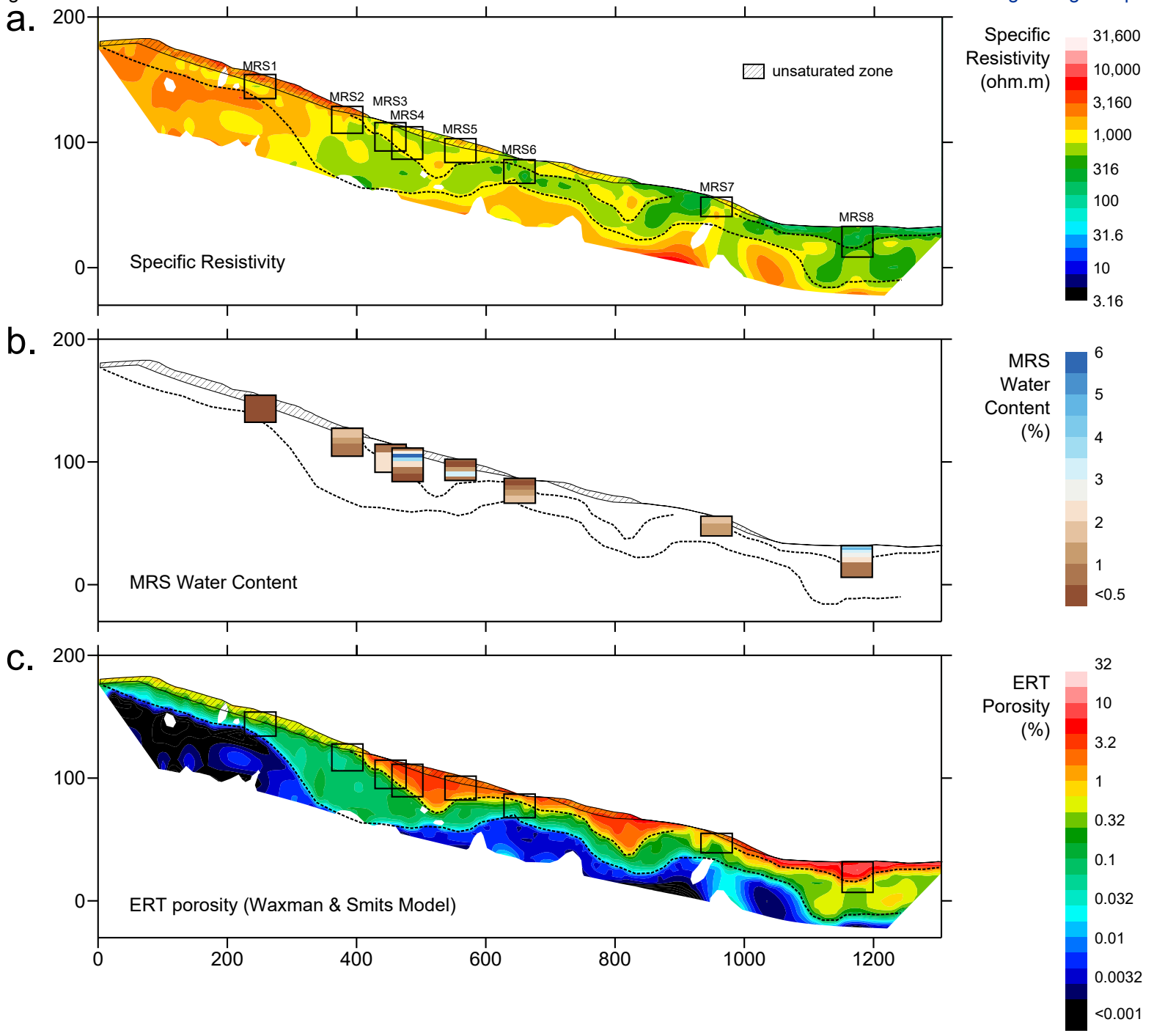

Figure 8

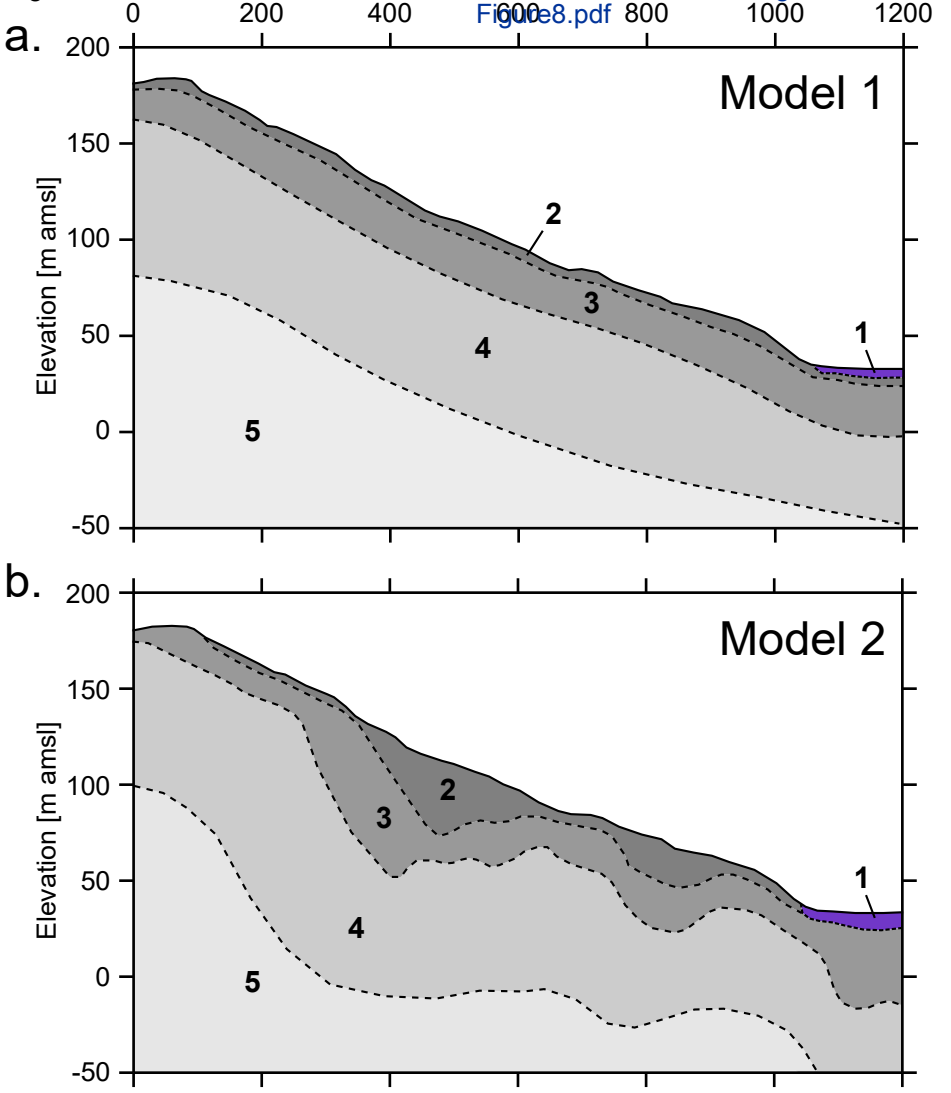

Figure 9

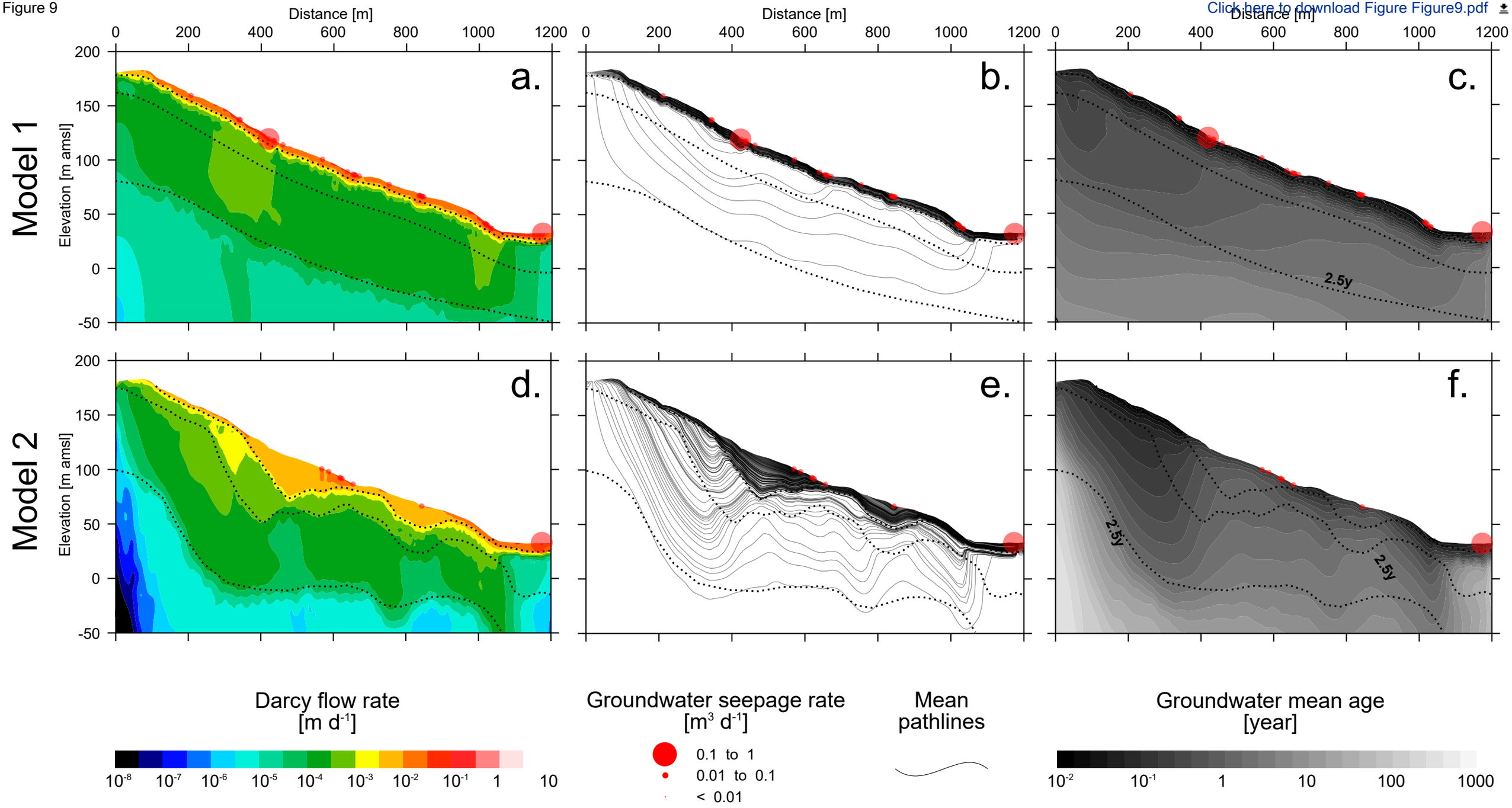

Figure 10

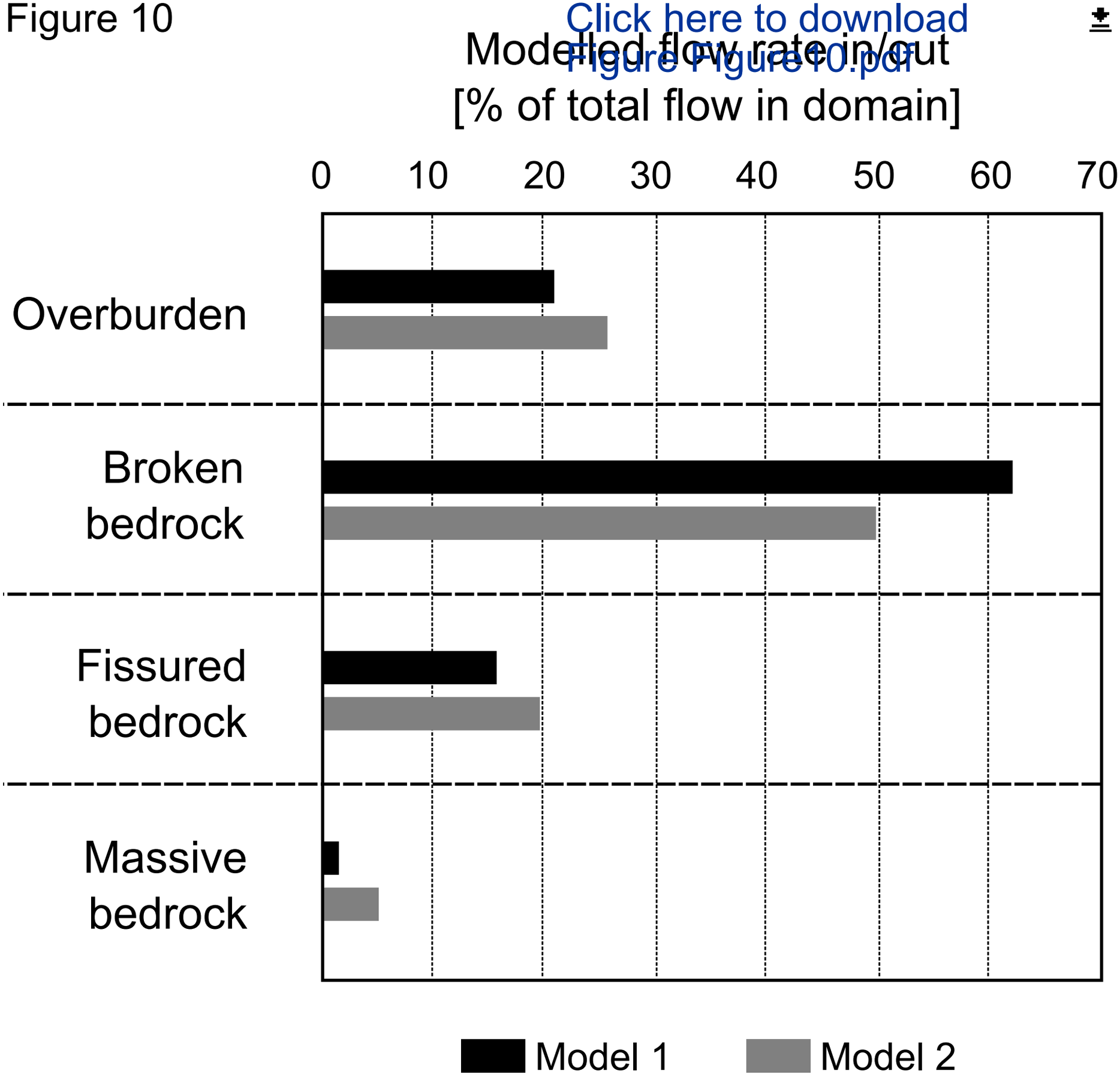

Figure 11